Comput. Methods Appl. Mech. Engrg. 270 (2014) 201–219

Contents lists available at ScienceDirect

Comput. Methods Appl. Mech. Engrg.

journal homepage: www.elsevier.com/locate/cma

A hybrid spectral and metamodeling approach for the stochastic finite element analysis of structural dynamic systems

A. Kundu [a,*], F.A. DiazDelaO [b], S. Adhikari [a], M.I. Friswell [a]

[a] Civil and Computational Engineering Centre, College of Engineering, Swansea University, Singleton Park, Swansea SA2 8PP, United Kingdom
[b] Institute for Risk and Uncertainty, School of Engineering, University of Liverpool, Brownlow Hill, Liverpool L69 3GH, United Kingdom

ARTICLE INFO

Article history:
Received 3 December 2012
Received in revised form 12 November 2013
Accepted 18 November 2013
Available online 7 December 2013

Keywords:
Stochastic finite element method
Stochastic structural dynamics
Spectral method
Bayesian emulation
Uncertainty analysis
Composite corrugated panels

ABSTRACT

A novel approach for uncertainty propagation and response statistics estimation of randomly parametrized structural dynamic systems is developed in this paper. The frequency domain response of a stochastic finite element system is resolved at randomly sampled design points in the input stochastic space with an infinite series expansion using preconditioned stochastic Krylov bases. The system response is expressed in the eigenvector space of the structural system weighted with finite order rational functions of the input random variables, termed spectral functions. The higher the order of the spectral functions, the more accurate is the order of approximation of the stochastic system response. However, this increased accuracy comes at a computational cost. This cost is mitigated by using a Bayesian metamodel. The proposed approach is used to the analyze the stochastic vibration response of a corrugated panel with random elastic parameters. The results obtained with the proposed hybrid approach are compared with direct Monte Carlo simulations, which have been considered as the benchmark solution.

1. Introduction

Uncertainty analysis of large engineering systems has received increasing attention over the past few years. This has called for efficient uncertainty propagation methods to be used for the stochastic mathematical models. The present work focuses on the parametric uncertainty of the constitutive system equations which may be either epistemic or aleatoric in nature [1]. This multiplicative stochasticity associated with randomly parametrized systems has been tackled with various methods ranging from the non-intrusive statistical simulation methods (such as the crude Monte Carlo simulation (MCS) and its variants [2]) to non-statistical analytical methods which provide explicit functional relationships between the independent random variables used to model the problem (such as the perturbation methods, the Neumann expansion method and the Galerkin-based finite order chaos expansion methods).

The various non-intrusive Monte Carlo Simulation techniques (in conjunction with advanced sampling and/or interpolation schemes) which have been analyzed and used in context of structural dynamics problems, can be found in [3]. Non-intrusive techniques enable the use of the already existing deterministic codes to solve the stochastic problem at carefully chosen sample points. Hence, there is no necessity to modify the deterministic solvers and adapt them to the stochastic case, it only involves constructing some post-processing routines. Also, the deterministic solvers working independently of each other at various sample points are trivially parallelizable. However, the convergence of the crude MCS is slow and the error

* Corresponding author.
E-mail address: a.kundu.577613@swansea.ac.uk (A. Kundu).
URL: http://engweb.swan.ac.uk/~kundua/ (A. Kundu).

0045-7825/$ - see front matter © 2013 Elsevier B.V. All rights reserved.
http://dx.doi.org/10.1016/j.cma.2013.11.013

converges as $\mathcal{O}\left(\frac{1}{\sqrt{N}}\right)$. The computational efficacy of these sample-based techniques can be substantially improved by reducing the problem to important random variables using principal component analysis and various efficient variance reduction techniques such as importance sampling, the multi-point estimate method, stratified sampling, and Latin hypercube sampling [4]. The limitations of these techniques are dictated by the input stochastic space dimension. However, uncertain structural systems represented by few random variables subjected to deterministic loading can be well-suited to variance reduction procedures.

The non-statistical methods, on the other hand, can provide an explicit functional relationship between the independent input random variables and hence allow easy evaluation of the functional statistics or probabilities of the stochastic system response. These approaches can be based on a perturbation method [5], or equivalently the lower-order Taylor approximation and the Neumann expansion method, [6] all of which come down to the estimation of the response surface in a parameter space. On the other hand, the Galerkin-type orthogonal projection methods [7] developed with different choices of the approximation space, systematically lead to a high precision solution allowing the response to be expressed explicitly in terms of the basic random variables describing the uncertainties. Their principal drawback lies in the fact that the dimensionality of the resulting system of linear equations is high. The Wiener–Hermite expansions in conjunction with the finite element (FE) methods have been widely applied to different problems [8,9]. It was extended to generalized polynomial chaos [10], which has provided an optimal convergence of the solution using the so-called Askey scheme.

The present work is concerned with uncertainty propagation methods and estimation of the response statistics of a class of stochastic partial differential equation commonly encountered in structural dynamic problems. An alternative solution methodology for the resolution of the frequency domain response of randomly parametrized structural dynamic systems is proposed here. The stochastic system response is expressed as a series expansion using the basis functions of a left-preconditioned stochastic Krylov space. This gives a set of highly non-linear finite order stochastic rational functions of the input random variables, termed as the *spectral functions*, which are used to express the solution in a reduced modal space. The higher the order of these spectral functions, the better is the precision of the approximated solution. This, however, results in greater computational cost. In order to mitigate this cost, we compute a statistical approximation to the system output. This metamodeling strategy, known as Gaussian process emulation [11], is based on the analysis and design of computer experiments ([12,13]) and on the concepts of Bayesian statistics. The non-expensive approximation to the output is made after evaluating a small number of points in the input space, hence reducing the required computer processing time. After conditioning on these training runs and updating a prior distribution, the mean of the resulting posterior distribution approximates the output of the simulator at any untried input, whereas it reproduces the known output at each design point. Gaussian process emulation has been implemented in various scientific fields with encouraging results. These fields include structural dynamics ([14]), multi-scale analysis ([15]), stochastic finite elements ([16]), and domain decomposition ([17]) among many others.

For many aerospace applications, different aeroelastically unstable structures often have inherent uncertainty in their parametric variables which can not be reduced despite repeated and strenuous measurements or expensive simulations. It is required to quantify these uncertainties and incorporate them into the mathematical model in terms of a finite dimensional stochastic field. These form the stochastic input space of the mathematical model. Propagating this input randomness of the physical system to the response quantities (such as displacement, pressure, velocity) can be tackled with various techniques, some of which has been outlined above. We analyze here a corrugated panel which is of significant potential in morphing aerospace structures largely due to the very high compliance it offers along the corrugation direction. The elastic parameters (such as the bending and elastic stiffness) of this panel have been considered as random fields and its effect on the stochastic response statistics have been analyzed.

The paper is organized as follows. Section 2 discusses the stochastic and spatial discretization associated with the weak formulation of the random physical problem and the existing solution techniques for the stochastic FE problems. Section 3 offers the theoretical foundations behind the construction of the proposed spectral function method. Section 4 contains an overview of Bayesian emulators and uncertainty analysis. In section 5 we discuss the computational complexity of the proposed hybrid method against crude Monte Carlo. In section 6 we apply the hybrid spectral and metamodeling approach to the uncertainty analysis of a corrugated panel. Section 7 provides conclusions developed from the current work.

2. Overview of the spectral stochastic finite element method

2.1. Randomly parametrized structural dynamic systems

Consider a damped randomly parametrized structural dynamic system, defined on the domain $\mathcal{D} \subset \mathbb{R}^d$ $(d \leqslant 3)$, with piecewise Lipschitz boundary $\partial\mathcal{D}$, subject to an externally applied deterministic excitation f_0. The equilibrium condition gives the following stochastic partial differential equation (SPDE)

$$\rho \frac{\partial^2 u}{\partial t^2} + \mathfrak{L}_\eta \frac{\partial u}{\partial t} + \operatorname{div}(\sigma_a(u)) = f_0 \quad \text{on } \mathcal{D},\ t \in \mathbb{R}^+, \tag{1}$$

with the associated Dirichlet boundary condition

$$u = 0 \quad \text{on } \partial\mathcal{D},$$

where $\sigma_a(u)$ is the stress related to the displacement field u, ρ is the mass density, and t is the time. $\mathfrak{Q}_\eta$ denotes the damping operator, with η as the damping parameter, and it can be used to represent different damping models such as the strain rate dependent viscous damping or the velocity dependent viscous damping. $(\Theta, \mathcal{F}, P)$ is a probability space where $\theta \in \Theta$ is a sample point from the sampling space Θ, $\mathcal{F}$ is the associated Borel σ-algebra and P is a probability measure. The constitutive equations relating the stress field to the displacement u is given as

$$\sigma_a(u) = a(\mathbf{r}, \theta) : \varepsilon(u),$$

where a is the Hooke's elasticity tensor and is a second order, stationary, square integrable random field such that $a : \mathbb{R}^d \times \Theta \to \mathbb{R}$. Here ':' denotes the standard tensor inner product of second order tensors. Depending on the physical problem, the random field $a(\mathbf{r}, \theta)$ can be used to model different physical systems.

For the harmonic analysis of the system Eq. (1) is written in the frequency domain (using Fourier transformation) as

$$-\omega^2 \rho \widetilde{u} + i\omega(\mathfrak{Q}_\eta \widetilde{u}) + \mathrm{div}(\sigma_a(\widetilde{u})) = \widetilde{f}_0(\omega), \quad \omega \in \Omega, \tag{2}$$

where Ω denotes the frequency space of the problem. Here $\widetilde{f}_0(\omega)$ and $\widetilde{u}(\omega)$ are the frequency dependent complex amplitudes of the harmonic input excitation and the system response, respectively.

2.2. Discretization of the parametric random field

The random parameter $a(\mathbf{r}, \theta) : \mathcal{D} \times \Theta$ is written in a series expandable form following a spectral decomposition of the covariance kernel as

$$\int_{\mathcal{D}} C_a(\mathbf{r}_1, \mathbf{r}_2)\varphi_j(\mathbf{r}_1)\mathrm{d}\mathbf{r}_1 = \nu_j \varphi_j(\mathbf{r}_2), \quad \forall j = 1, 2, \ldots. \tag{3}$$

The above is a homogeneous Fredholm integral equation of the second kind. If $\mathcal{C}_a\varphi$ is defined as $(\mathcal{C}_a\varphi)(\mathbf{r}_2) = \int_{\mathcal{D}} C_a(\mathbf{r}_1, \mathbf{r}_2)\varphi(\mathbf{r}_1)d\mathbf{r}_1, \quad \mathbf{r}_1, \mathbf{r}_2 \in \mathbb{R}^d$, it can be verified that $\mathcal{C}_a : L^2(\mathbb{R}^d) \to L^2(\mathbb{R}^d)$ is a linear operator on a vector space. Hence Eq. (3) can be expressed as $\mathcal{C}_a\varphi = \nu\varphi$. A non-trivial solution to the above homogeneous equation exists only for those values of ν which make $(I - \nu\mathcal{C}_a)$ singular, where I is the identity operator. The covariance functions C_a are usually bounded and symmetric, hence the associated linear operator $\mathcal{C}_a$ is compact and self-adjoint. The solution of the eigenvalue problem in 3 yields ordered real eigenvalues $\nu = \{\nu_i : \nu_i \geqslant \nu_{i+1}\ \forall i \text{ and } \|C_a\|^2_{L^2(\mathbb{R}^d \times \mathbb{R}^d)} = \sum_i \nu_i^2\}$ and mutually orthogonal eigenfunctions $\varphi(\mathbf{r}_1)$ in $L^2(\mathbb{R}^d)$. Thus, from Mercer's theorem we can write

$$C_{a_M}(\mathbf{r}_1, \mathbf{r}_2) = \sum_{i=1}^{M} \nu_i \varphi(\mathbf{r}_1)\varphi(\mathbf{r}_2), \tag{4}$$

where C_{a_M} converges uniformly to C_a as $M \to \infty$.

Using the above results, the random field can be represented with a denumerable set of eigenvalues and eigenvectors of the covariance kernel using the Karhunen–Loève (KL) expansion as

$$a(\mathbf{r}, \theta) = a_0(\mathbf{r}) + \sum_{i=1}^{M} \sqrt{\nu_i}\,\widetilde{\xi}_i(\theta)\varphi_i(\mathbf{r}), \tag{5}$$

where $a_0(\mathbf{r}) = \mathbb{E}[a(\mathbf{r}, \theta)]$ is the mean, and $\widetilde{\xi}_i(\theta)$ are the mutually independent random variables with zero mean $(\mathbb{E}[\widetilde{\xi}_i] = 0)$ and unit variance $(\mathbb{E}[\widetilde{\xi}_i{}^2] = 1)$ for $i = 1, \ldots, M$. The above expansion is valid for Gaussian random fields. General non-Gaussian random fields are expressed in a mean-square convergent series using the Wiener–Askey chaos expansion scheme [10], where the basis functions are constructed with a denumerable set (M) of independent random variables $\boldsymbol{\xi} = [\xi_1, \xi_2, \ldots, \xi_M]^{\mathsf{T}} \in \Theta^{(M)}$ where $\Theta^{(M)} \subset \Theta$. These basis functions span the stochastic Hilbert space and hence the problem can be equivalently formulated on a finite dimensional probability space $(\Theta^{(M)}, \mathcal{F}^{(M)}, P^{(M)})$ where $\Theta^{(M)} = \mathrm{Range}(\boldsymbol{\xi})$, $\mathcal{F}^{(M)}$ is the associated Borel σ-algebra and $P^{(M)}$ is a probability measure. The formulation presented in this paper is applicable to this kind of general decomposition of the random field.

2.3. Finite element analysis of the discretized random system

The FE treatment of the governing SPDE involves spatial discretization of the continuum $\mathcal{D} \in \mathbb{R}^d$ into domains with polygonal boundaries $\mathcal{D}^h$ where h is the mesh space parameter is presented here. It is known from the Doob–Dynkin lemma [18] that for the parametrized equation in Eq. (1), where the input randomness is expressed in terms of a finite dimensional vector $\boldsymbol{\xi}(\theta)$ (as in 5), the solution can be expressed entirely in terms of the same random variables. Thus the solution of the discretized FE system is sought in the Hilbert space $\mathcal{H}(\mathcal{D}^h \times \Theta)$. This space can be expressed in a separable form with the Hilbert spaces $\mathcal{H}_1$ and $\mathcal{H}_2$ such that $\mathcal{H} \simeq \mathcal{H}_1 \otimes \mathcal{H}_2$. Following this, the well established techniques of variational formulation of the displacement-based deterministic finite-element method gives us the following form of the stochastic system matrices [9,7,19] using the discretization technique illustrated in Section 2.2. The system matrices inherit the randomness of the input stochastic parameters and hence the stochastic linear system for structural dynamics takes the form of

$$\left[-\omega^2\mathbf{M}(\theta)+j\omega\mathbf{C}(\theta)+\mathbf{K}(\theta)\right]\widetilde{\mathbf{u}}(\omega,\theta)=\widetilde{\mathbf{f}}_0(\omega),$$
$$\text{or,}\quad \left(\mathbf{A}_0(\omega)+\sum_{i=1}^{M}\xi_i(\theta)\mathbf{A}_i(\omega)\right)\widetilde{\mathbf{u}}(\omega,\theta)=\widetilde{\mathbf{f}}_0(\omega), \tag{6}$$

where $\mathbf{M}(\theta),\mathbf{C}(\theta)$ and $\mathbf{K}(\theta)$ are the random mass, damping and stiffness matrices, respectively, which have been combined to obtain the complex frequency dependent coefficient matrices $\mathbf{A}_i(\omega),\ i=0,1,\ldots,M$. Also,

$$\mathbf{M}(\theta)=\mathbf{M}_0+\sum_{i=1}^{p_1}\mu_i(\theta)\mathbf{M}_i\in\mathbb{R}^{n\times n}\quad\text{and}\quad\mathbf{K}(\theta)=\mathbf{K}_0+\sum_{i=1}^{p_2}\nu_i(\theta)\mathbf{K}_i\in\mathbb{R}^{n\times n}. \tag{7}$$

Here ($\mathbf{M}_0$ and $\mathbf{K}_0$) are the deterministic mass and stiffness matrices while ($\mathbf{M}_i$ and $\mathbf{K}_i$) are the corresponding perturbation components obtained from discretizing the mass and stiffness parameters with finite number of random variables ($\mu_i(\theta)$ and $\nu_i(\theta)$). The total number of random variables utilized to represent the stochastic system matrices is $M=p_1+p_2$. We have chosen the proportional damping model in the present work where the damping parameter is expressed as a linear combination of the mass matrix and the system stiffness matrix.

For the proportional damping model considered here $\mathbf{C}(\theta)=\zeta_1\mathbf{M}(\theta)+\zeta_2\mathbf{K}(\theta)$, where ζ_1 and ζ_2 are deterministic scalars. Hence the expressions for the coefficient matrices are given by

$$\mathbf{A}_0(\omega)=\left[-\omega^2+j\omega\zeta_1\right]\mathbf{M}_0+[j\omega\zeta_2+1]\mathbf{K}_0, \tag{8}$$
$$\text{and, }\mathbf{A}_i(\omega)=\left[-\omega^2+j\omega\zeta_1\right]\mathbf{M}_i\quad\text{for}\quad i=1,2,\ldots,p_1, \tag{9}$$
$$\mathbf{A}_k(\omega)=[j\omega\zeta_2+1]\,\mathbf{K}_k\quad\text{for}\quad k=p_1+1,p_1+2,\ldots,p_1+p_2,$$

The solution methodologies of the system given in Eq. (6) is presented in the following section.

2.4. Spectral methods and other solution techniques

Several approaches exist for the solution of the randomly parametrized structural dynamic system of the form given in Eq. (6). A first approach known as the *modal approach* involves the solution of the random eigenvalue problem. The random eigenvalues can be obtained using various approaches such as polynomial chaos [20], asymptotic integral [21] and sensitivity based approaches [22]. The system in Eq. (6) is a system of coupled, complex stochastic linear algebraic equations. For real valued equations, several methods have been proposed which include, first- and second-order perturbation methods [5], the Neumann expansion method [6] and simulation methods [2]. Another class of methods which has been used widely in the literature is known as the spectral Galerkin methods. These include the polynomial chaos (PC) expansion [9], generalized spectral decomposition technique [23] and Wiener–Askey chaos expansion [10]. Methods based on the projection of the stochastic system response on to a reduced stochastic Krylov space has been studied in [24]. Lastly, More recently a reduced spectral function method has been proposed which provides a numerically efficient way of resolving the response of stochastic structural dynamic systems [25].

For the calculation of the frequency response function (FRF) of dynamical systems, several approaches, such as metamodels based methods[26], interpolation based methods [27], modal approaches [28] and the Approximate Principal Deformation Mode (APDM) approach [29] have been proposed.

In the present context, it is found that the random matrices $\mathbf{A}:\Theta\to\mathbb{C}^{n\times n}$ and $\widetilde{\mathbf{f}}_0:\Theta\to\mathbb{C}^n$ in Eq. (6) inherit the continuity and coercivity properties from the governing SPDE through the weak formulation. Thus, it can be said that, the spatially discretized solution vector $\widetilde{\mathbf{u}}(\omega,\theta)$ lies in the tensor product space $\mathbb{C}^n\otimes\Upsilon$, where Υ is an ad-hoc function space for real-valued random variables. Given that the stochastic system has been discretized and represented with a finite number of random variables $\hat{\boldsymbol{\xi}}(\theta)=[\hat{\xi}_1,\ldots,\hat{\xi}_p]^{\mathrm{T}}$ as in Section 2.2, the stochastic subspace reduces to Υ_p where $\Upsilon_p\subset\Upsilon$. When each random component $\hat{\xi}^{(i)}$ is independent, then Υ_p is a tensor product space $\Upsilon^1\otimes\Upsilon^2\otimes\ldots\otimes\Upsilon^p$. According to the approximate basis building techniques that focus on expansion of the solution vector using some polynomial functions, the solution vector in Eq. (6) can be expressed in the form

$$\widetilde{\mathbf{u}}(\omega,\theta)=\sum_{\alpha\in\mathcal{I}_p}\mathcal{H}_\alpha(\theta)\widetilde{u}_\alpha(\omega);\quad\widetilde{u}_\alpha(\omega)\in\mathbb{C}^n, \tag{10}$$

where $\mathcal{H}_\alpha$ are the basis in Υ_p and $\widetilde{u}_\alpha(\omega)$ are the set of complex frequency dependent unknown coefficients to be evaluated.

The form of the polynomial functions $\mathcal{H}_\alpha(\omega,\theta)$ used in Eq. (10) varies according to the chosen solution approach. The spectral approaches (polynomial chaos, generalized chaos) classically use orthogonal polynomial basis $\mathcal{H}_\alpha(\theta)$ to approximate the solution in stochastic space such that the latter is expressed as a mean-square convergent series. Thus the classical spectral Galerkin approximation techniques of solving the stochastic system using a finite number of stochastic basis can be posed as follows: it is necessary to find $\widetilde{u}_\alpha(\omega)\in\mathbb{C}^n\otimes\Upsilon_p$ such that

$$\sum_{\alpha\in\mathcal{I}_p}E(\mathbf{A}\mathcal{H}_\beta\mathcal{H}_\alpha)\widetilde{u}_\alpha=E(\mathcal{H}_\beta\widetilde{\mathbf{f}}_0)\quad\forall\,\beta\in\mathcal{I}_p, \tag{11}$$

which leads to a set of linear algebraic equations to evaluate the unknown coefficients introduced in Eq. (10). The above solution methodology is applicable for the whole range of stochastic spectral function approaches to solve non-deterministic systems. Frequency domain analysis of stochastic systems has been studied using this method [30] for the medium-frequency structural dynamic analysis. However, the computational cost of solving the linear system obtained from Eq. (11) can become high for systems with large dimensionality and near resonance frequencies even for moderate values of variability of the input random field. Some Krylov-type iterative resolution techniques [31,32] have been established which takes advantage of the sparsity of the system and tries to employ a preconditioner to efficiently solve a given system. However, the availability of optimal preconditioners is limited to systems with low variance and hence for other systems, the iterative technique results in a drastic increase in computational costs.

As a result, several methods have been developed (see for example [33]) which aim at reducing the computational cost. It is observed that for the polynomial chaos based solution approach, the stochastic space is spanned with orthogonal polynomials which are constructed based on the probability density function of the random variables *only*. However, in context of the discretized finite element systems, more information, such as the deterministic system matrices and their perturbation components, are also available. The classical orthonormal basis for the PC method are not dependent on frequency, which may lead to the solution being non-convergent near resonance frequencies and/or certain standard deviations of the random parameter, or requiring a very high number of basis vectors at some frequencies compared to others, indicating the need for adaptivity. Adaptive generalized polynomial chaos has been implemented to tackle long-term integration for stochastic advection-diffusion problems in [34]. It may be possible to realize an alternative solution strategy dependent on the specific problem at hand and utilizing the information of the random system matrices to formulate a good approximation of the stochastic coefficients $\mathcal{H}_\alpha(\omega,\theta)$ in Eq. (10). This is the motivation behind the solution technique proposed here.

3. Stochastic finite elements and the spectral function approach

The efficiency of the stochastic finite element method is governed by the accuracy with which the solution can be approximated using fewer number of terms in the stochastic series expansion. A reference to the idea of stochastic Krylov space is relevant in this context and can help the representation of the response vector in a reduced subspace that can alleviate much of the computational burden. A Krylov subspace projection approach in conjunction with Galerkin technique has been proposed in [24]. We also refer to the work in [25], which proposed a reduced spectral function approach for parabolic stochastic systems using the eigenvectors of the baseline model as the basis vectors. The underlying idea in the present work is to find the solution of a randomly parametrized linear system as an infinite series expansion using stochastic Krylov basis functions whose dimension is the degree of the minimal polynomial of the system matrices.

Let $\mathbf{Ax}=\mathbf{b}$ be a non-singular linear algebraic system. The solution vector $\mathbf{x}$ of this equation lies in the mth order Krylov subspace as

$$\mathcal{K}_m(\mathbf{A},\mathbf{b}) = \text{span}\{\mathbf{b},\mathbf{Ab},\mathbf{A}^2\mathbf{b},\ldots,\mathbf{A}^{m-1}\mathbf{b}\}. \tag{12}$$

The Krylov subspace dimension, however, is a key factor affecting the computational efficacy of a proposed approach. It follows that the solution of the stochastic linear systems (in Eq. (6)), can be projected on to a finite number of basis spanning a *stochastic* Krylov space

$$\mathcal{K}_m\left[\underbrace{\left(\mathbf{A}_0(\omega)+\sum_{i=1}^{M}\xi_i(\theta_i)\mathbf{A}_i(\omega)\right)}_{\mathbf{A}(\omega,\theta)},\widetilde{\mathbf{f}}_0(\omega)\right]. \tag{13}$$

A choice of a finite number of Krylov basis depends on the eigenspectrum of the system matrix $\mathbf{A}(\omega,\theta)$. A reduction in the dimension of the Krylov subspace can be achieved if we use a preconditioned stochastic Krylov space to arrive at a richer stochastic subspace. The mean of the coefficient matrix has been employed as the preconditioner which helped in transforming $\mathbf{A}(\theta)$ such that the probability density functions of its eigenvalues show a high degree of overlap [24]. However, as the variability of the random field increases, a preconditioner devised with some of the randomness of the system matrices performs better so that the order of the spectral basis functions can be kept low.

The system matrices $\mathbf{K}_0$ and $\mathbf{M}_0$ are symmetric, non-negative definite, and the eigenvectors $\boldsymbol{\phi}_k\in\mathbb{R}^n,\ \forall k=1,2,\ldots n$ of the generalized eigenvalue problem,

$$\mathbf{K}_0\boldsymbol{\phi}_k=\lambda_k\mathbf{M}_0\boldsymbol{\phi}_k;\quad k=1,2,\ldots n \tag{14}$$

forms a complete basis. Taking a reduced number n_r of eigenpairs as $\boldsymbol{\lambda}_0=\text{diag}[\lambda_1,\lambda_2,\ldots,\lambda_{n_r}]$ and $\boldsymbol{\Phi}=\left[\boldsymbol{\phi}_1,\boldsymbol{\phi}_2,\ldots,\boldsymbol{\phi}_{n_r}\right]\in\mathbb{R}^{n\times n_r}$ to transform the stochastic linear system in Eq. (6) to the corresponding generalized modal coordinates we have

$$\begin{aligned}\boldsymbol{\Phi}^T\mathbf{A}_0\boldsymbol{\Phi} &= \boldsymbol{\Phi}^T\left([-\omega^2+i\omega\zeta_1]\mathbf{M}_0+[i\omega\zeta_2+1]\mathbf{K}_0\right)\boldsymbol{\Phi},\\ \text{or } \boldsymbol{\Phi}^T\mathbf{A}_0\boldsymbol{\Phi} &= \left(-\omega^2+i\omega\zeta_1\right)\mathbf{I}+(i\omega\zeta_2+1)\boldsymbol{\lambda}_0,\end{aligned} \tag{15}$$

$$\text{from which, } \boldsymbol{\Phi}^T\mathbf{A}_0\boldsymbol{\Phi}=\boldsymbol{\Lambda}_0 \quad\text{and}\quad \mathbf{A}_0=\boldsymbol{\Phi}^{-T}\boldsymbol{\Lambda}_0\boldsymbol{\Phi}^{-1}. \tag{16}$$

Here $\mathbf{\Lambda}_0 = (-\omega^2 + i\omega\zeta_1)\mathbf{I} + (i\omega\zeta_2 + 1)\lambda_0$ depends on the frequency step ω and the eigenvalue of the system. Introducing the transformation $\widetilde{\mathbf{A}}_i = \mathbf{\Phi}^T\mathbf{A}_i\mathbf{\Phi} \in \mathbb{C}^{n\times n}; i = 0, 1, 2, \ldots, M$, and its inverse $\mathbf{A}_i = \mathbf{\Phi}^{-T}\widetilde{\mathbf{A}}_i\mathbf{\Phi}^{-1} \in \mathbb{C}^{n\times n}$, we have

$$\widetilde{\mathbf{u}}(\omega,\theta) = \left[\mathbf{\Phi}^{-T}\mathbf{\Lambda}_0(\omega)\mathbf{\Phi}^{-1} + \sum_{i=1}^{M}\xi_i(\theta)\mathbf{\Phi}^{-T}\widetilde{\mathbf{A}}_i(\omega)\mathbf{\Phi}^{-1}\right]^{-1}\widetilde{\mathbf{f}}_0(\omega) = \mathbf{\Phi}\mathbf{\Psi}(\omega,\xi(\theta))\mathbf{\Phi}^T\widetilde{\mathbf{f}}_0(\omega), \tag{17}$$

where $\mathbf{\Psi}(\omega,\xi(\theta)) = \left[\mathbf{\Lambda}_0(\omega) + \sum_{i=1}^{M}\xi_i(\theta)\widetilde{\mathbf{A}}_i(\omega)\right]^{-1}$ and the M-dimensional random vector $\xi(\theta) = \{\xi_1(\theta), \xi_2(\theta), \ldots, \xi_M(\theta)\}^T$. $\widetilde{\mathbf{A}}_i$ is written as a sum of diagonal (Λ_i) and off-diagonal Δ_i (all diagonal elements set to 0) matrices as $\widetilde{\mathbf{A}}_i = \mathbf{\Lambda}_i + \mathbf{\Delta}_i,\ i = 1, 2, \ldots, M$. Thus $\mathbf{\Psi}(\omega,\xi(\theta)) = [\mathbf{\Lambda}(\omega,\xi(\theta)) + \mathbf{\Delta}(\omega,\xi(\theta))]^{-1}$.

We transform the stochastic system response to the modal coordinates as $\widetilde{\mathbf{u}}(\omega,\theta) = \sum_i \Phi_i c_i(\omega,\theta) = [\mathbf{\Phi}]\{\mathbf{c}_i(\omega,\theta)\}$, where $\mathbf{c}(\omega,\theta) \in \mathbb{C}^n$ is the complex, frequency dependent modal response vector and following from Eq. (17) and the previous discussions we have

$$[\mathbf{\Lambda}(\omega,\xi(\theta)) + \mathbf{\Delta}(\omega,\xi(\theta))]\mathbf{c}(\omega,\theta) = \mathbf{\Phi}^T\widetilde{\mathbf{f}}_0(\omega), \tag{18}$$

such that $\mathbf{c}(\omega,\theta) = [\mathbf{\Lambda}(\omega,\xi(\theta)) + \mathbf{\Delta}(\omega,\xi(\theta))]^{-1}\mathbf{\Phi}^T\widetilde{\mathbf{f}}_0(\omega) = \mathbf{\Psi}(\omega,\xi(\theta))\mathbf{\Phi}^T\widetilde{\mathbf{f}}_0(\omega)$. Referring back to Eq. (13), the diagonal matrix $\mathbf{\Lambda}(\omega,\xi(\theta))$ is treated as the preconditioner of the stochastic Krylov space. The diagonal dominance of the matrices $\widetilde{\mathbf{A}}_i(\omega)$ is conducive to the approach being proposed here. Also, it has been shown [35] that when the mean of the coefficient matrix is used as the preconditioner, the terms of the Neumann series also span the left preconditioned stochastic Krylov space. This can be readily extended to include the case of using $\mathbf{\Lambda}(\omega,\xi(\theta))$ as the preconditioner giving the stochastic system response (in the modal coordinates) in the m dimensional stochastic Krylov space as

$$\begin{aligned}\mathbf{c}(\omega,\theta) &\in \mathcal{K}_m\Big(\mathbf{\Lambda}^{-1}(\omega,\xi(\theta))[\mathbf{\Lambda}(\omega,\xi(\theta)) + \mathbf{\Delta}(\omega,\xi(\theta))], \mathbf{\Lambda}^{-1}(\omega,\xi(\theta))\mathbf{\Phi}^T\widetilde{\mathbf{f}}_0(\omega)\Big)\\ &\in \mathcal{K}_m\Big(\big[I + \mathbf{\Lambda}^{-1}(\omega,\xi(\theta))\mathbf{\Delta}(\omega,\xi(\theta))\big], \mathbf{\Lambda}^{-1}(\omega,\xi(\theta))\mathbf{\Phi}^T\widetilde{\mathbf{f}}_0(\omega)\Big).\end{aligned} \tag{19}$$

Utilizing the property of the Krylov subspace shift invariance [35] (which states that $\mathcal{K}_j(\alpha\mathbf{A} + \mathbf{I}, \mathbf{b}) = \mathcal{K}_j(\mathbf{A}, \mathbf{b})$ for any matrix $\mathbf{A}$, vector $\mathbf{b}$ and nonzero scalar α) we have from Eq. (19)

$$\mathbf{c}(\omega,\theta) \in \mathcal{K}_m\Big(\mathbf{\Lambda}^{-1}(\omega,\xi(\theta))\mathbf{\Delta}(\omega,\xi(\theta)), \mathbf{\Lambda}^{-1}(\omega,\xi(\theta))\mathbf{\Phi}^T\widetilde{\mathbf{f}}_0\Big), \tag{20}$$

which gives the Krylov subspace in which the stochastic system solution exists. The span of the Krylov space is then given by

$$\mathcal{K}_m(\mathbf{\Lambda}^{-1}\mathbf{\Delta}, \mathbf{\Lambda}^{-1}\mathbf{\Phi}^T\widetilde{\mathbf{f}}_0) = \text{span}\{\mathbf{\Lambda}^{-1}\mathbf{\Phi}^T\widetilde{\mathbf{f}}_0, (\mathbf{\Lambda}^{-1}\mathbf{\Delta})\mathbf{\Lambda}^{-1}\mathbf{\Phi}^T\widetilde{\mathbf{f}}_0, (\mathbf{\Lambda}^{-1}\mathbf{\Delta})^2\mathbf{\Lambda}^{-1}\mathbf{\Phi}^T\widetilde{\mathbf{f}}_0, \ldots, (\mathbf{\Lambda}^{-1}\mathbf{\Delta})^{m-1}\mathbf{\Lambda}^{-1}\mathbf{\Phi}^T\widetilde{\mathbf{f}}_0\} \tag{21}$$

It can be seen that the basis functions of the left-preconditioned Krylov space obtained in Eq. (21) are equal to the terms of an *equivalent Neumann series expansion* and hence a series solution of Eq. (18). Thus the coefficients of the left-preconditioned Krylov basis functions are not evaluated using a Galerkin-type projection scheme but rather from the equivalent Neumann series expansion. Combining Eqs. (17)–(21) the modal response vector can then be expressed in an equivalent Neumann series using the m stochastic Krylov basis functions as

$$\mathbf{c}(\omega,\theta) = \sum_{s=0}^{m-1}(-1)^s\left(\mathbf{\Lambda}^{-1}\mathbf{\Delta}\right)^s\mathbf{\Lambda}^{-1}\mathbf{\Phi}^T\widetilde{\mathbf{f}}_0(\omega) = \mathbf{\Gamma}^{(m)}(\omega,\xi(\theta)), \tag{22}$$

where $\mathbf{\Gamma}^{(m)}(\omega,\xi(\theta)) = \{\Gamma_1^{(m)}(\omega,\xi(\theta)), \ldots, \Gamma_n^{(m)}(\omega,\xi(\theta))\}^T$ is the vector of complex frequency dependent stochastic coefficients and hence the arbitrary rth element of the stochastic response vector $\widetilde{\mathbf{u}}(\theta)$ approximated with mth order stochastic spectral functions, is given by

$$\widetilde{u}_r^{(m)}(\omega,\theta) = \sum_{k=1}^{n_r}\Gamma_k^{(m)}(\omega,\xi(\theta))\boldsymbol{\phi}_{r,k}. \tag{23}$$

Thus the solution vector $\widetilde{\mathbf{u}}(\theta)$ is projected in the space spanned by $\boldsymbol{\phi}_k$ and weighted by $\Gamma_k^{(m)}(\omega,\xi(\theta))$ which would be referred to as mth order spectral functions in this article.

This preconditioning (used in Eq. (21)) provides substantial advantage over the classical Neumann series expansion. In the latter case, the deterministic part of the system matrices are used as preconditioners and it results in the series becoming non-convergent near the resonance frequencies. This is easy to explain when considering the fact that the spectral radius of the inverse of the deterministic system is much greater than 1 near the resonance frequencies and hence the matrix power series fails to converge.

Definition 1. $\Gamma_k^{(m)}(\omega,\xi(\theta)), k = 1, 2, \ldots n$ are termed as mth order *spectral functions* characterized by the spectral properties of the system matrices and are frequency dependent rational functions of the input random variables.

In the spectral Galerkin approaches and the Neumann type expansions, the stochastic system response solution is projected onto *polynomial* functions of the input random variables. In contrast, the series in Eqs. (22) and (23) is in terms of $[\mathbf{\Lambda}^{-1}(\omega,\xi(\theta))][\mathbf{\Delta}(\omega,\xi(\theta))]$, where both terms are random. The convergence of this series depends on the spectral radius of

$$\mathbf{R}(\omega,\boldsymbol{\xi}(\theta)) = \boldsymbol{\Lambda}^{-1}(\omega,\boldsymbol{\xi}(\theta))\boldsymbol{\Delta}(\omega,\boldsymbol{\xi}(\theta)). \tag{24}$$

The elements of this matrix series are not simple polynomials in $\xi_i(\theta)$, but are in terms of a ratio of polynomials as follows

$$R_{rs} = \frac{\Delta_{rs}}{\Lambda_{rr}} = \frac{\sum_{i=1}^{M}\xi_i\Delta_{i_{rs}}}{\Lambda_{0_r}+\sum_{i=1}^{M}\xi_i\Lambda_{i_r}} = \frac{\sum_{i=1}^{M}\xi_i\widetilde{A}_{i_{rs}}}{\Lambda_{0_r}+\sum_{i=1}^{M}\xi_i\widetilde{A}_{i_{rr}}}; \quad r\neq s. \tag{25}$$

Eq. (25) shows that the spectral radius of $\mathbf{R}$ is controlled by the diagonal dominance of $\widetilde{\mathbf{A}}_i$, i.e. if the diagonal terms are relatively larger than the off-diagonal terms, the series will converge faster even if the relative magnitude of Λ_{0_r} is not large. Especially near the resonance frequencies, when the deterministic system is nearly singular, the classical Neumann expansion fails to converge altogether. Hence the diagonal parts of the perturbation matrices have a significant role to play in this improved solution technique. For the discretized finite element structural systems, the assembled global system matrices are diagonally dominant. Thus the series can be said to converge surely as the order m of spectral functions is increased.

Lemma 1. *If $\widetilde{\mathbf{u}}^{(m)}(\omega,\boldsymbol{\xi}(\theta))$ is the approximate solution constructed with mth order spectral functions and $\widetilde{\mathbf{u}}(\omega,\boldsymbol{\xi}(\theta))$ is the exact solution of $\mathbf{A}\widetilde{\mathbf{u}} = \widetilde{\mathbf{f}}_0$, where $A:\mathbb{R}^n\to\mathbb{R}^n$ is self-adjoint, then the error in the approximate solution for each random sample is bounded by*

$$\|\widetilde{\mathbf{u}} - \widetilde{\mathbf{u}}^{(m)}\| \leqslant c_\phi\sum_{k=m}^{\infty}\rho(\mathbf{R})^k\|\Lambda^{-1}\boldsymbol{\Phi}^T\widetilde{\mathbf{f}}_0\|, \tag{26}$$

where $\mathbf{A} = \Lambda + \Delta$, $\rho(\mathbf{R})$ is the spectral radius of $\mathbf{R} = (\Lambda^{-1}\Delta)$, $\|\cdot\|$ denotes the 2-norm and c_ϕ is a deterministic, frequency independent positive constant.

Proof. When the solution $\widetilde{\mathbf{u}}^{(m)}$, approximated with mth order spectral functions $\Gamma^m(\omega,\boldsymbol{\xi}(\theta))$, is subtracted from $\widetilde{\mathbf{u}}$, we can write (from Eqs. (22) and (23)) the difference as $\boldsymbol{\Phi}\left(\sum_{k=m}^{\infty}(-\mathbf{R})^k\Lambda^{-1}\boldsymbol{\Phi}^T\widetilde{\mathbf{f}}_0\right)$. Hence from the Cauchy–Schwartz inequality and using the triangle inequality we have

$$\|\widetilde{\mathbf{u}} - \widetilde{\mathbf{u}}^{(m)}\| \leqslant \|\boldsymbol{\Phi}\|\left\|\sum_{k=m}^{\infty}(-\mathbf{R})^k\Lambda^{-1}\boldsymbol{\Phi}^T\widetilde{\mathbf{f}}_0\right\| \leqslant \sum_{k=m}^{\infty}\|\mathbf{R}^k(\Lambda^{-1}\boldsymbol{\Phi}^T\widetilde{\mathbf{f}}_0)\|\|\boldsymbol{\Phi}\|.$$

We define $\rho(\mathbf{R}) = max_j(|\lambda_{R_j}|)$ to be the spectral radius of $\mathbf{R}$, (λ_R being the eigenvalue of $\mathbf{R}$) and note that $\mathbf{R}$ is symmetric. We know from Gelfand's formula that $\lim k\to\infty\left\|\mathbf{R}^k\right\|^{1/k} = \rho(\mathbf{R})$ and from [36] it is seen that for any general matrix sets $\gamma^{(1+\ln k)/k}\left\|\mathbf{R}^k\right\|^{1/k} \leqslant \rho(\mathbf{R}) \leqslant \left\|\mathbf{R}^k\right\|^{1/k}$ where $\gamma\in(0,1)$. When using the 2-norm and as k increases, $\rho(\mathbf{R})$ approaches $\left\|\mathbf{R}^k\right\|^{1/k}$ such that we can approximate $\left\|\mathbf{R}^k\right\| = c_\rho\rho(\mathbf{R})^k$ where $c_\rho\to 1$. The norm of the orthonormalized matrix $\boldsymbol{\Phi}$ is $\sqrt{n}$ where n is the dimension of the linear system. We choose $c_\phi = \sqrt{n}c_\rho$ which is a deterministic, frequency independent positive constant. Hence, the above equation can be rewritten as

$$\|\widetilde{\mathbf{u}} - \widetilde{\mathbf{u}}^{(m)}\| \leqslant c_\phi\sum_{k=m}^{\infty}\rho(\mathbf{R})^k\|\Lambda^{-1}\boldsymbol{\Phi}^T\widetilde{\mathbf{f}}_0\|. \tag{27}$$

Thus the approximation error for stochastic system solution approximated with mth order spectral function converges with the mth power of the spectral radius of $\mathbf{R}$. □

For $\rho(\mathbf{R})\ll 1$ and square-integrable stochastic functions $\rho(\mathbf{R})^k$ and $\|\Lambda\|$ in the probability space $\left(\Theta^{(M)},\mathcal{F}^{(M)},P^{(M)}\right)$, with $\theta\in\Theta^{(M)}$, the expectation of the error norm can be written from Lemma 1 and using Hölder's inequality, as

$$\mathbb{E}[\|\widetilde{\mathbf{u}}^{(m)} - \widetilde{\mathbf{u}}\|] \leqslant \mathcal{O}(\langle\rho(\mathbf{R})^m\rangle_{L^2(\theta)})c(\omega), \tag{28}$$

where $c(\omega) = \langle c_\phi\|\Lambda^{-1}\boldsymbol{\Phi}^T\widetilde{f}_0\|\rangle_{L^2(\theta)} \leqslant c_\phi\|\boldsymbol{\Phi}^T\widetilde{f}_0\|\langle\|\Lambda^{-1}\|\rangle_{L^2(\theta)}$ is a constant that changes with the frequency step. Here $\langle\cdot\rangle_{L^2(\theta)}$ denotes the 2-norm in the probability space defined as $\left(\int_{\Theta^{(M)}}|\cdot|^2\,dP_\xi^{(M)}(\theta)\right)^{1/2}$ or $\mathbb{E}[|\cdot|^2]^{1/2}$. Thus the series converges rapidly as the order m of the spectral functions is increased.

The spectral functions used in the approximation of the stochastic system response are highly non-linear in $\boldsymbol{\xi}(\theta)$ indicating that the response vector is a non-linearly filtered version of the random variables used to model the parametric uncertainty. For structural mechanics problems, the eigenvectors $\boldsymbol{\phi}_k$ are vibrational modes and Eq. (23) indicates that the response of a stochastic system is a linear combination of fundamental vibration modes weighted by the stochastic spectral functions Γ_k.

The above development is not restricted to any specific choice of the joint distribution function of the input random variables. $\widetilde{\mathbf{u}}^{(m)}(\omega,\theta)$ is the solution of Eq. (6) for a sufficiently large value of m. The choice of the order of spectral functions m is guided by the desired accuracy of the solution and the consideration of computational efficacy. Hence, the series in Eq. (23) approaches the exact solution of the discretized linear stochastic system Eq. (6) for every $\theta\in\Theta$, $\omega\in\Omega$ as $m\to\infty$ as shown

in Lemma 1. Thus it converges with probability 1. Here we present Algorithm 1 which summarizes the proposed spectral function approach. It is noted that this algorithm is applied at every $\omega \in \Omega$.

Algorithm 1. Stochastic FEM analysis using spectral functions

Input: Frequency $\omega \in \Omega$, n design points : $\{\xi^{(1)}, \ldots, \xi^{(n)}\} \subset \Theta^{(M)}$.
Input: KL modes $\varphi_i(\mathbf{r}_1) \mapsto \int_{\mathbb{R}^d} C_a(\mathbf{r}_1, \mathbf{r}_2)\varphi_i(\mathbf{r}_2)d\mathbf{r}_2$, system matrices $\widetilde{\mathbf{A}}_i$, $i = 0, \ldots, M$.
Input: First few eigenpairs from $\mathbf{K}_0\boldsymbol{\phi}_k = \lambda_k \mathbf{M}_0\boldsymbol{\phi}_k$.
Output: Approximate stochastic system response vector $\widetilde{\mathbf{u}}^{(m)}(\theta, \omega) \in \mathbb{R}^n \times \Theta$.
1: **for** j = 1 to n **do**
2: Evaluate the Krylov left-preconditioner $\boldsymbol{\Lambda}^{-1}(\omega, \xi(\theta))$.
3: Form the preconditioned linear system $(\boldsymbol{\Lambda}^{-1}\boldsymbol{\Delta})$ and $\mathbf{b} = (\boldsymbol{\Lambda}^{-1}\boldsymbol{\Phi}^T\widetilde{\mathbf{f}}_0)$
4: **for** r = 1 to m **do**
5: Evaluate the successive powers of $(\boldsymbol{\Lambda}^{-1}\boldsymbol{\Delta})^r$.
6: Construct the Krylov basis following Eq. (21) using $(\boldsymbol{\Lambda}^{-1}\boldsymbol{\Delta})^r$ and $\mathbf{b}$.
7: **end for**
8: Create mth order spectral functions $\{\boldsymbol{\Gamma}^{(m)}(\omega, \xi(\theta))\}$ from series expansion in Eq. (22).
9: Reconstruct the system response $\widetilde{\mathbf{u}}^{(m)}(\xi^{(j)}(\theta), \omega)$ using Eq. (23).
10:**end for**
GLOBALS $\{(\xi^{(i)}, \widetilde{\mathbf{u}}^{(m)}(\xi^{(i)}, \omega))|i = 1, \ldots, n\}$ %{Pass to Algorithm 2}

4. Metamodeling approach

In Eq. (23), we showed that the response vector $\widetilde{\mathbf{u}}^{(m)}$ at each frequency step ω is a approximated with a finite order rational function of the stochastic variables $\xi(\theta)$. In this section, we briefly review a metamodeling strategy to cope with the computational cost of obtaining a statistical summary of the response. Let $\hat{u}_k^{(m)}(\xi(\theta), \omega)$ be the kth component of the response vector $\widetilde{\mathbf{u}}^{(m)}$ evaluated at the design point $\xi(\theta)$. If the response vector $\widetilde{\mathbf{u}}^{(m)}$ is evaluated at n design points $\xi^{(1)}(\theta), \ldots, \xi^{(n)}(\theta)$, then a vector $\widehat{\mathbf{u}}_k^{(m)} = (\hat{u}_k^{(m)}(\xi^{(1)}(\theta), \omega), \ldots, \hat{u}_k^{(m)}(\xi^{(n)}(\theta), \omega))^{\mathsf{T}}$ is obtained. In order to simplify the notation, we make the dependence on θ and ω implicit and re-express $\widehat{\mathbf{u}}_k^{(m)}$ as $\widehat{\mathbf{u}}_k^{(m)} = (\hat{u}_k^{(m)}(\xi^{(1)}), \ldots, \hat{u}_k^{(m)}(\xi^{(n)}))^{\mathsf{T}} \in \mathbb{R}^n$.

4.1. Bayesian emulation

For an input $\xi = (\xi_1, \ldots, \xi_p)^{\mathsf{T}}$, the kth component of the global response calculated by Algorithm 1 is a scalar $\hat{u}_k^{(m)}(\xi)$. The cost of running the code makes it affordable to evaluate only a limited number of design points $\xi^{(1)}, \ldots, \xi^{(n)}$ when using high order spectral functions. The uncertainty about the output that arises due to this cost can be modeled probabilistically. To that effect, let the vector $\widetilde{\mathbf{u}}^{(m)}$ of observed outputs be realizations of a Gaussian stochastic process. The model structure for a single component of the output vector is thus expressed as

$$\hat{u}_k^{(m)}(\xi) = \mathbf{h}(\xi)^{\mathsf{T}}\boldsymbol{\beta} + Z(\xi), \tag{29}$$

where $\mathbf{h}(\xi)$ is a vector of known functions and $\boldsymbol{\beta}$ is an unknown hyperparameter to be estimated from the data. The choice of $\mathbf{h}(\xi)$ is an active research area. Some authors ([37,45]) point out that it should be chosen to reflect the available information about the functional form of the output, and that whenever possible, it is worth investing as much effort as possible modeling this mean function. In this paper we choose a constant mean and delegate the responsibility of capturing complex relationships to the function $Z(\cdot)$. This function is a stochastic process with mean zero and covariance function

$$Cov(Z(\xi), Z(\xi')) = \sigma_z^2 C(\xi, \xi'), \tag{30}$$

where $C(\xi, \xi')$ is a correlation function and σ_z^2 is the process variance, a hyperparameter that can also be estimated from the data. In order to choose a valid positive-definite correlation function, some authors ([12]) consider products of one-dimensional correlations, specifically functions of the form

$$C(\xi, \xi') = \prod_{i=1}^{n} \exp\left\{-b_i(\xi_i - \xi_i')^2\right\}, \tag{31}$$

where $b_i > 0$ for all i. This correlation function is infinitely differentiable, which is convenient to incorporate derivative information ([38]). The vector of smoothness hyperparameters $\mathbf{b} = (b_1, \ldots, b_n)^{\mathsf{T}}$ quantifies the rate at which the output varies as the input varies. Intuitively, the less smooth the output, the more strongly will it respond to small changes in the input. The above prior knowledge can be summarized in a prior probability distribution of the form

$$\hat{u}_k^{(m)}(\xi)|\boldsymbol{\beta},\sigma_z^2,\mathbf{b}\sim\mathcal{N}(\mathbf{h}(\xi)^\top\boldsymbol{\beta},\sigma_z^2C(\xi,\xi')). \tag{32}$$

Let $\mathcal{D}=\{(\xi^{(i)},\hat{u}_k^{(m)}(\xi^{(i)}))|i=1,\ldots,n\}$ be the set of training runs corresponding to the kth component of the global finite element solution provided by Algorithm 1. Given this observed dataset, Bayes' theorem is used to estimate the hyperparameters [39,40]. Once this is done, the prior distribution in Eq. (32) is updated and the mean of the resulting posterior distribution approximates the output $\hat{u}_k^{(m)}(\xi^*)$ at any untried input ξ^*, whereas it interpolates the observed output at the design points $\xi^{(1)},\ldots,\xi^{(n)}$. At the same time, the variance of the posterior distribution quantifies the uncertainty that arises from the limited availability of code evaluations ([41]) due to computational cost. The resulting posterior distribution is of the form

$$\hat{u}_k^{(m)}(\xi)|\widehat{\mathbf{u}}_k^{(m)},\boldsymbol{\beta},\sigma_z^2\sim\mathcal{N}(m^*(\xi),\sigma_z^2C^*(\xi,\xi')), \tag{33}$$

where the posterior mean and posterior variance are such that

$$m^*(\xi)=\boldsymbol{\beta}+\mathbf{r}(\xi)^\top\mathbf{R}^{-1}(\widehat{\mathbf{u}}_k^{(m)}-\mathbf{1}\boldsymbol{\beta}), \tag{34}$$

$$C^*(\xi,\xi')=\mathbf{R}(\xi,\xi')-\mathbf{r}(\xi)^\top\mathbf{R}^{-1}\mathbf{r}(\xi'). \tag{35}$$

In the above expressions, $\mathbf{R}\in\mathbb{R}^{n\times n}$ with $[\mathbf{R}]_{ij}=C(\xi^{(i)},\xi^{(j)})$; $\mathbf{r}(\xi)\in\mathbb{R}^n$ such that $\mathbf{r}(\xi)=\left(C(\xi,\xi^{(1)}),\ldots,C(\xi,\xi^{(n)})\right)^\top$; and $\mathbf{1}\in\mathbb{R}^n$ such that $\mathbf{1}=(1,\ldots,1)^\top$. The posterior mean $m^*(\cdot)$ provides is a fast approximation of the output $\hat{u}_k^{(m)}(\xi)$ for any ξ in the input domain.

Since it could be difficult to specify $\boldsymbol{\beta}$ and σ_z^2, they can be integrated out in order to obtain the posterior distribution of $\hat{u}_k^{(m)}(\xi)|\widetilde{\mathbf{u}}^{(m)},\sigma_z^2$. That way, the posterior distribution becomes

$$\hat{u}_k^{(m)}(\xi)\|\widehat{\mathbf{u}}_k^{(m)},\sigma_z^2\sim\mathcal{N}(m^{**}(\xi),\sigma_z^2C^{**}(\xi,\xi')), \tag{36}$$

with

$$m^{**}(\xi)=\widehat{\boldsymbol{\beta}}+\mathbf{r}(\xi)^\top\mathbf{R}^{-1}(\widehat{\mathbf{u}}_k^{(m)}-\mathbf{1}\widehat{\boldsymbol{\beta}}), \tag{37}$$

$$C^{**}(\xi,\xi')=C^*(\xi,\xi')+\left(1-\mathbf{r}(\xi)^\top\mathbf{R}^{-1}\mathbf{1}\right)\left(\mathbf{1}^\top\mathbf{R}^{-1}\mathbf{1}\right)^{-1}\left(1-\mathbf{r}(\xi')^\top\mathbf{R}^{-1}\mathbf{1}\right)^\top, \tag{38}$$

$$\widehat{\boldsymbol{\beta}}=(\mathbf{1}^\top\mathbf{R}^{-1}\mathbf{1})^{-1}\mathbf{1}^\top\mathbf{R}^{-1}\widehat{\mathbf{u}}_k^{(m)}. \tag{39}$$

Finally, σ_z^2 can also be integrated out in order to obtain:

$$\frac{\hat{u}_k^{(m)}(\xi)-m^{**}(\xi)}{\widehat{\sigma}_z\sqrt{C^{**}(\xi)}}\sim t_{n-1}, \tag{40}$$

where

$$\widehat{\sigma}_z^2=\frac{\widehat{\mathbf{u}}_k^{(m)\top}\left(\mathbf{R}^{-1}-\mathbf{R}^{-1}\mathbf{1}(\mathbf{1}^\top\mathbf{R}^{-1}\mathbf{1})\mathbf{1}^\top\mathbf{R}^{-1}\right)\widehat{\mathbf{u}}_k^{(m)}}{n-2}, \tag{41}$$

which is a Student's t-distribution with $n-1$ degrees of freedom.

Algorithm 2. Bayesian emulation

Input: Training runs $\mathcal{D}=\left\{\left(\xi^{(i)},\hat{u}_k^{(m)}(\xi^{(i)})\right)|i=1,\ldots,n\right\}$ % {From Algorithm 1}

Output: Posterior mean $m^*(\xi)$ and posterior covariance $C^*(\xi,\xi')$

1: Obtain the hyperparameters' posterior distribution $\mathcal{P}(\boldsymbol{\beta},\sigma_z^2,\mathbf{b}|\mathcal{D})=\frac{\mathcal{P}(\mathcal{D}|\boldsymbol{\beta},\sigma_z^2,\mathbf{b})\mathcal{P}(\boldsymbol{\beta},\sigma_z^2,\mathbf{b})}{\mathcal{P}(\mathcal{D})}$

2: Update the prior in Eq. (32) to obtain the posterior $\hat{u}_k^{(m)}(\xi)|\widehat{\mathbf{u}}_k^{(m)},\sigma_z^2$ in Eq. (36)

3: Compute $m^{**}(\xi)$ from Eq. (37) and $C^{**}(\xi,\xi')$ from Eq. (38) % {Pass to Algorithm 3}

4.2. Bayesian uncertainty analysis

A finite element code, such as the one considered in this paper, is deterministic. This means that if it is run repeatedly at the same input ξ, it will always return the same output $\hat{u}_k^{(m)}(\xi)$. However, the inputs we are interested in are physical parameters, the values of which are uncertain. The aim of uncertainty analysis is to propagate the uncertainty in the inputs through the S code in order to characterize the distribution of the output, which is itself a random variable $\mathbf{Y}$. The first stage of the uncertainty analysis is to quantify the uncertainty in the inputs by specifying a probability distribution $\mathcal{F}(\xi)$. If the code were not computationally expensive, the most straightforward uncertainty analysis would proceed by drawing a large sample

$\{\xi^{(1)}, \ldots, \xi^{(N)}\}$ from the input distribution $\mathcal{F}(\xi)$ and then running the code at each realization. This would result in an output sample from which any statistic or summary $\mathbb{S}(\mathbf{Y})$ can be estimated. $\mathbb{S}(\mathbf{Y})$ could be the mean, the variance, a particular percentile, or any other summary.

A simple way to carry out uncertainty analysis would be to directly replace the code with the emulator's posterior mean $m^{**}(\xi)$ in Eq. (36). Potentially, this predictive mean can be evaluated a large number of times at any untried input at very low cost. However, this approach would not incorporate the fact that $m^{**}(\xi)$ is itself an inexact approximation to the output and hence it introduces additional uncertainty. To circumvent this problem, an approach proposed in [42,43] is employed and the strategy is detailed in Algorithm 3.

Agorithm 3. Uncertainty analysis using a GPE

Input: Posterior mean $m^{**}(\xi)$, and posterior covariance $C^{**}(\xi, \xi')$ % {From Algorithm 2}
Input: Large sample $\left\{\xi^{(1)}, \ldots, \xi^{(N)}\right\}$ from the input distribution $\mathcal{F}(\xi)$,
Output: Summary $\mathbb{S}(\mathbf{Y})$ of the output distribution $\mathbf{Y}$
1: $\boldsymbol{\mathcal{S}} \leftarrow \varnothing$
2: Draw a large sample $\{\xi^{(1)}, \ldots, \xi^{(N)}\}$ from the distribution $\mathcal{F}(\xi)$
3: **for** j = 1 to K **do**
4: Draw a random function $y_{(j)}$ from the posterior distribution 36
5: Evaluate $y_{(j)}(\xi^{(1)}), \ldots, y_{(j)}(\xi^{(N)})$
6: Obtain $\mathbb{S}_j(\mathbf{Y})$, the Monte Carlo estimate of $\mathbb{S}(\mathbf{Y})$
7: $\boldsymbol{\mathcal{S}} \leftarrow \boldsymbol{\mathcal{S}} \cup \mathbb{S}_j(\mathbf{Y})$
8: **end for**
9: Use $\boldsymbol{\mathcal{S}}$ to estimate any summary of the distribution of $\mathbb{S}(\mathbf{Y})$

For illustration of the complete process, Fig. 1 shows ten iterations of Algorithm 3 for a toy model, with ξ uniformly distributed in the interval $[-5, 5]$. The training runs are generated by a simulator using Algorithm 1, then emulation is performed by Algorithm 2 to compute the posterior mean and variance, and finally the uncertainty distribution is generated by Algorithm 3.

5. Algorithmic complexity

The improvement in efficiency of the proposed hybrid spectral and metamodeling technique over the crude Monte Carlo simulation is presented here in light of the algorithmic complexity of the two methods. The improvement is due to the use of finite order spectral functions within the framework of finite dimensional Krylov space, the use of a reduced number of orthogonal basis functions in constructing the stochastic system response, and solving the random system at only a few design points in the stochastic input space.

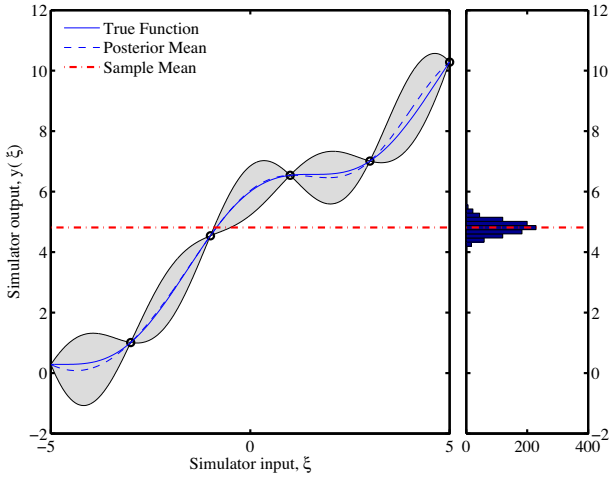

Fig. 1. Illustration of the uncertainty analysis: the posterior mean (dotted curve) approximates the true output (solid curve) based on a few training runs (circles). The code inputs are random variables uniformly distributed as $\xi \sim U(-5, 5)$. 95% credible intervals are also shown (shaded areas). Note how the uncertainty in the training runs is zero, since the true output is known. The mean of each random function drawn from the posterior distribution results in a realization of the sample mean, the distribution of which can be approximated (histogram) and a statistical summary estimated.

Let n_{dof} be the dimension of the complete stochastic finite element linear system and let N_s be the number of Monte Carlo samples. Then, the total computational complexity at each frequency step is $N_s\mathcal{O}(n_{\text{dof}}^3)$. For the spectral method, the calculation of various orders of spectral functions requires the evaluation of $\mathbf{\Lambda}^{-1}(\omega,\boldsymbol{\xi}(\theta))\mathbf{\Delta}(\omega,\boldsymbol{\xi}(\theta))$ in Eq. (20), whose complexity is $\mathcal{O}(n_{\text{dof}}^2)$. Hence, the pth order spectral function has a complexity of $(p-1)\mathcal{O}(n_{\text{dof}}^2)$. Summing up all the computations required for calculating the m-dimensional stochastic Krylov basis (as shown in Eq. (21)), and given that the successive basis can be obtained recursively from the previous basis, the computational complexity is $N_s m\mathcal{O}(n_{\text{dof}}^2)$ for the solution of system at all the N_s samples. We can see that the calculation of the finite order spectral functions is almost one order of magnitude less than that of the crude Monte Carlo. However, for most of the low to mid frequency structural dynamic problems, a good approximation of the vibration response is obtained by considering only the first few eigenpairs. If we adopt this reduced system, then the dimension of the linear system is reduced to n_r where $\boldsymbol{\lambda}_0 = \text{diag}[\lambda_1,\lambda_2,\ldots,\lambda_{n_r}]$ and $\mathbf{\Phi} = [\boldsymbol{\phi}_1,\boldsymbol{\phi}_2,\ldots,\boldsymbol{\phi}_{n_r}]$. The complexity involved in this case for the calculation of the pth order spectral function would be $(p-1)\mathcal{O}(n_r^2)$. Hence, when constructing the system response using m-dimensional stochastic Krylov basis and a reduced number of orthogonal eigenmodes, the complexity is given by $N_s m\mathcal{O}(n_r^2)$, where $n_r \ll n_{\text{dof}}$. In the worst case scenario, if very high degrees of spectral functions are considered, such that $m \approx n_r$, the complexity becomes $N_s\mathcal{O}(n_r^3)$.

While the spectral approach is efficient in reducing the complexity of solving the linear system at the stochastic points, the metamodel is used to mitigate the cost of solving an $\mathcal{O}(n_r^3)$ complex system at each one of the N_s samples. Hence, n design points (with $n \ll N_s$) are chosen using a sampling plan (such as a Latin hypercube) and the stochastic system response is calculated to generate training runs. This results in the complexity being reduced further to $nm\mathcal{O}(n_r^2)$. Given these n training runs, the complexity of emulating the response is $\mathcal{O}(n^3)$. This is due to the linear system solved in Eqs. (37) and (38), where $\mathbf{R} \in \mathbb{R}^{n\times n}$. Therefore, the complexity of the hybrid approach is the sum of the complexity associated with the generation of the training runs with the spectral method plus the complexity of the emulator. The above discussion is summarized in Table 1. The resolution of the eigenvalue problem required for the spectral method is done only once in the beginning and is stored and used in the subsequent steps of the algorithm. Iterative Krylov subspace methods (like the Arnoldi's method or Lanczos algorithm) are employed for this purpose since the system matrices in structural dynamic systems are sparse, symmetric and positive definite. The number of iterations required for the convergence of the required number of eigenpairs is driven by the condition number of the system. Also, the determination of the first few eigenpairs of large sparse finite element systems is amenable to efficient parallelization and has been implemented in libraries such as ARPACK [44]. Hence the evaluation of the eigenpairs do not enhance the order of computational complexity associated with the Spectral method given in Table 1.

It is worth mentioning that the cost associated with the estimation of the hyperparameters can become prohibitive, especially for a large n. However, if the code that is emulated is very expensive, only a few training runs might be available. This might render the cost of estimating the hyperparameters relatively negligible. Naturally, the problem with having only few training runs undermines the predictive capability of any metamodel. It is therefore the task of the investigator to keep a balance between computational cost and robustness of the metamodel. If the Bayesian metamodel presented here becomes non-robust, a possible alternative is the linear Bayes approach [45]. Rather than calculate a full posterior distribution for the model output, this approach assesses just the posterior mean and variance. Additionally, this approach can be combined with implausibility measures in order to rapidly exclude areas of the input domain in which fits are unlikely to be found.

We give here briefly an estimation of the computational times obtained with the proposed method and its comparison with the MCS method. We assume that the FE linear system is of dimension 6630 and that the solution with the spectral function approach has been approximated with 4th order spectral functions and 200 eigen modes of the baseline structural system. This choice is justified by the fact that the analysis is being carried out within the frequency bandwidth of 0–300 Hz and the chosen modes satisfactorily capture the deformation shapes within this frequency range. The average time taken for 10,000 sample direct MCS simulation at each frequency step using matrix factorization method is found to be $\approx 2.4\times10^4$ s while the same for the 4th order spectral method is 374 s (assuming that the eigen modes have been precomputed). When the Biconjugate Gradient method is used to take advantage of the sparse FE system with an incomplete LU decomposition of the system matrix as the preconditioner the computational time for resolving 10,000 sample solutions comes down to $\approx$5000 s. It is to be mentioned that the Biconjugate Gradient solver is optimized to use the BLAS libraries for performing parallel matrix–vector operations on 8 computational cores of identical capability. On the other hand, when 125 samples are solved training runs are generated to be used as training runs for the emulation, the cost for the 4th order spectral method comes down to 6s and the cost of emulation is 50 s. This shows that the computational efficacy of the proposed spectral function method with Bayesian metamodeling is significantly efficient when compared with brute force MCS technique with and without sparse solvers.

Table 1
Computational complexity of the proposed hybrid approach against crude Monte Carlo for each frequency level. The number of samples is such that $n \ll N_s$. The number of degrees of freedom is given by n_{dof}. The reduced number of modes is n_r. The order of the spectral functions, and hence the number of Krylov bases, is given by m.

Method	Complexity	No. samples
Crude Monte Carlo	$N_s\mathcal{O}(n_{\text{dof}}^3)$	N_s
Spectral method	$N_s m\mathcal{O}(n_r^2)$	N_s
Spectral method + emulation	$nm\mathcal{O}(n_r^2)+\mathcal{O}(n^3)$	n

6. Application: dynamic analysis of a corrugated panel

6.1. Corrugated panel

The ability of an aircraft wing to change its geometry during flight has interested researchers and designers over the years [46]. This capability could have important practical advantages: by using smart morphing structures, significant reductions in fuel consumption and drag could be obtained. By helping flow laminarization, the lift to drag ratio could be increased. Moreover, the capability of a morphing wing could enable optimization of the aerodynamic performance not only for a single flight condition but during the entire mission. The use of flaps and slats are a simplification of the idea behind morphing. Unfortunately, conventional hinged mechanisms are not efficient, as the hinges and junctions create discontinuities in the surface that result in undesirable fluid dynamic phenomena such as flow separation and turbulence. One of the problems that remains to be solved is the design of suitable morphing skins [47]. Such skins have conflicting requirements:

1. Compliance in the chordwise direction to allow shape change and increase the surface area.
2. Stiffness in the spanwise direction to enable the aerodynamic and inertial loads to be carried.

Corrugated laminates offer a plausible solution for morphing aircraft skins due to their extremely anisotropic behavior. The corrugation direction (chordwise direction) offers compliance and the spanwise direction (transverse to corrugation) makes the structure much stiffer.

6.2. Stochastic modeling

We consider the problem of structural vibration of a corrugated panel with random parameters. Corrugated panels are prone to geometric uncertainties (due to manufacturing) or material uncertainties, such as a random bending stiffness. We choose this last example to demonstrate the effectiveness of the hybrid spectral and metamodeling approach proposed. We analyze a composite corrugated panel similar to the one presented in [48]. Fig. 2(a) shows a sketch of the unit cell with the corresponding geometry. Fig. 2(b) shows the meshed geometry of the corrugated panel that has been employed in the analysis. The panel's Young's modulus is taken as 16 GPa and its Poisson's ratio as 0.225. We applied the proposed computational approach to the corrugated panel, modeling it to be simply-supported at the ends (pinned at one end and a roller at the other). We have applied proportional Rayleigh damping for the present analysis. The frequency range of interest of the problem is 0–300 Hz. As mentioned above, we assumed the elastic parameters such as the bending stiffness and the axial stiffness of the plate to be random. We model these parameters as the stationary Gaussian random field

$$\alpha(\mathbf{r}, \xi(\theta)) = \alpha_0(1 + \epsilon(\mathbf{r}, \xi(\theta))), \tag{42}$$

where α is the random parameter of the corrugated panel, $\mathbf{r}$ is the length along the physical dimensions of the corrugated panel and $\epsilon(\mathbf{r}, \xi(\theta))$ is a zero mean stationary Gaussian random field. It might be mentioned that the Gaussian random field model, strictly speaking, might not be always physically meaningful since the elastic parameters being modeled are positive. However, if the number of KL expansion terms is chosen carefully then it is possible to show that the truncated statistical models are strictly positive [49]. We have chosen the baseline isotropic Young's modulus to be 16 GPa. The autocorrelation function of this random field has been assumed to be exponential. Thus if $\mathbf{r}_1 \neq \mathbf{r}_2$ then

$$C_\epsilon(\mathbf{r}_1, \mathbf{r}_2) = \sigma_\epsilon \exp\left\{-(|\mathbf{r}_1 - \mathbf{r}_2|)/\mu_\mathbf{r}\right\}, \tag{43}$$

where $\mu_\mathbf{r}$ is the correlation length defined along the physical dimensions of the panel and σ_ϵ is the standard deviation associated with the random elastic parameters. For the finite element model, the panel has been modeled with plate elements allowing uniaxial bending deformation and in-plane stretching deformation. The corrugated panel has been meshed with a uniform mesh defined by a mesh parameter size of $h = 0.98$ mm. The correlation length used in the autocorrelation model in

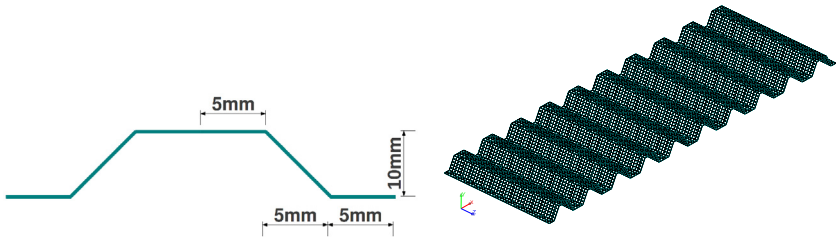

(a) Sketch of one corrugated unit (b) Meshed corrugated panel

Fig. 2. Model of the corrugated panel employed in the analysis. (a) Unit cell; (b) finite element model of the corrugated panel. The dimensions are: 300 mm in length, 75 mm in width, and 10 mm in height.

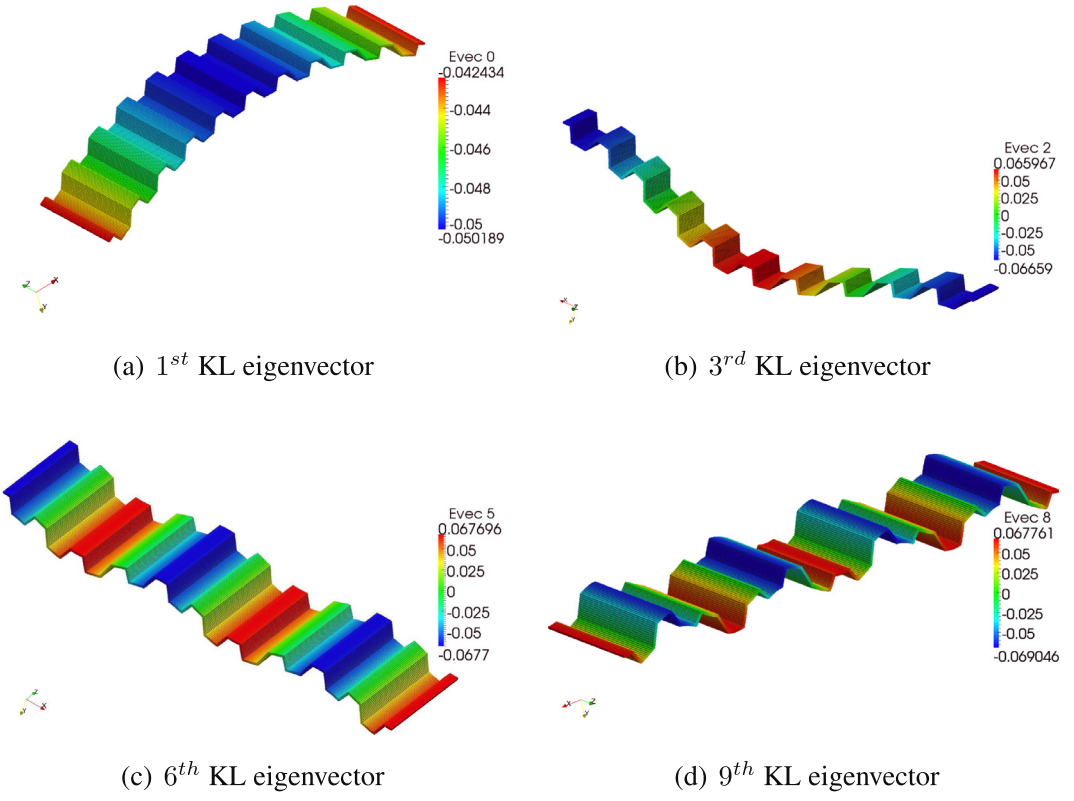

Fig. 3. Four different eigenvectors from the KL expansion of the random elastic parameter for the exponential covariance kernel with a correlation length of $L/2$, where L is the dimension of the physical domain. The eigenfunctions have been plotted as the out-of-plane displacements of the panel to graphically highlight their nature.

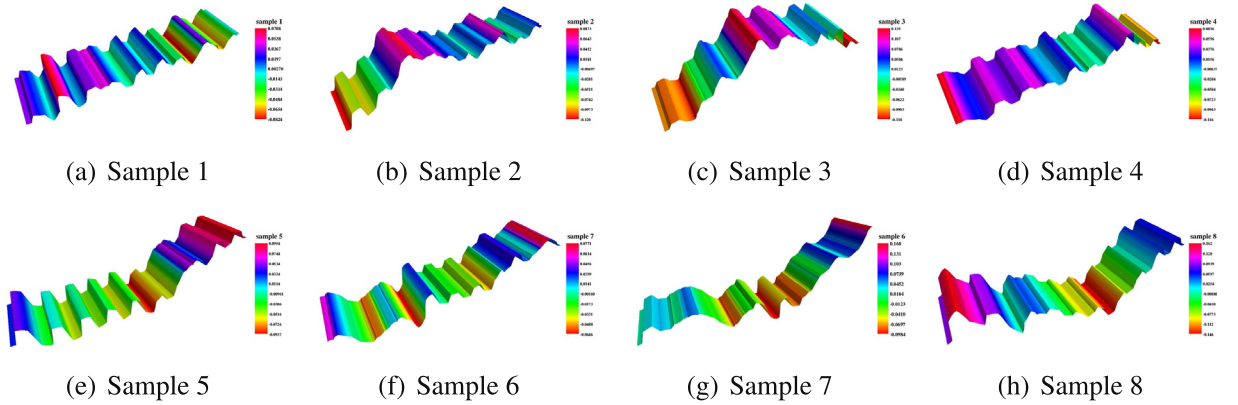

Fig. 4. Samples of the random elastic parameter plotted as the out-of-plane displacement of the corrugated panel to graphically highlight their nature. The correlation length has been chosen as $L/2$, where L is the dimension of the physical domain. The input standard deviation of the random field is 0.1.

Eq. (43) has been chosen as half of the principal geometric length of the panel. Fig. 3 shows a few chosen eigenvectors associated with the KL expansion of the covariance kernel. Note that the random elastic parameters and the KL eigenmodes are scalar quantities over the spatial domain. In order to facilitate better graphical representation of these quantities, they have been plotted as out-of-plane (y-direction) displacements of the panel. It shows that the higher modes are more complicated in shape which is similar to the behavior of higher structural vibrational modes. However, it must be noted that these KL modes are not the same as the vibrational modes of the structural finite element system.

Fig. 4 presents the sample realization of the random field constructed with a finite dimensional expansion (25 terms in this case) of the covariance function with a set of independent identically distributed (iid) Gaussian random variables. The

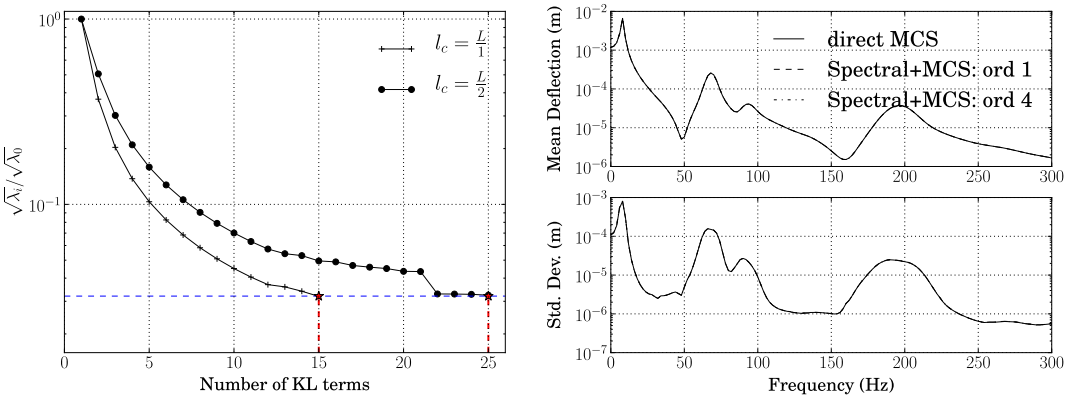

(a) The eigenvalue spectrum of the Covariance kernel

(b) The mean and standard deviation of the FRF of the plate

Fig. 5. (a) The decay of the eigenvalue spectrum of the exponential covariance kernel of the corrugated plate for different correlation lengths defined as the $L2$ norm. (b) The mean and standard deviation of the FRF of the center node of the plate calculated with the different orders of the spectral function approach with 10,000 stochastic sample simulations.

random variables have been sampled using a Latin-hypercube design from the input stochastic space of 25 random variables. The standard deviation of the random field is taken to be 0.1.

In order to decide the number of terms in the KL expansion, the eigenspectrum associated with the exponential covariance function is shown in Fig. 5(a) for two different correlation lengths $L/1$ and $L/2$ where L is the dimension of the physical domain of the problem. It is seen that the eigenvalues decay more rapidly for the larger correlation lengths indicating that fewer number of KL modes can capture most of the variability of the exponential kernel. For the stochastic vibration response analysis in the remainder of this work, we have chosen the correlation length to be $L/2$ and hence approximated the random field with the most dominant 25 modes of the expansion. This sets the dimension of the input stochastic space and 25 iid random variables were used to represent the discretized random elastic parameters in the spatial domain. The standard deviation of the random field was assumed to be $\sigma_\epsilon = 0.1$.

Fig. 5(b) shows the typical mean and standard deviation of the frequency response function of the center node of the corrugated panel subjected to unit amplitude harmonic out-of-plane force along the centerline of the plate over a frequency range of 0–300 Hz in steps of 2 Hz. The forcing vector is taken to be deterministic in nature. The plot presents a comparison of the second order statistics of the stochastic panel response calculated using the different orders (1 and 4) of spectral functions and with the direct MCS. A good agreement has been obtained. These response statistics have been obtained with a large sample size (10,000) and hence is computationally demanding. This cost would increase further if more accurate

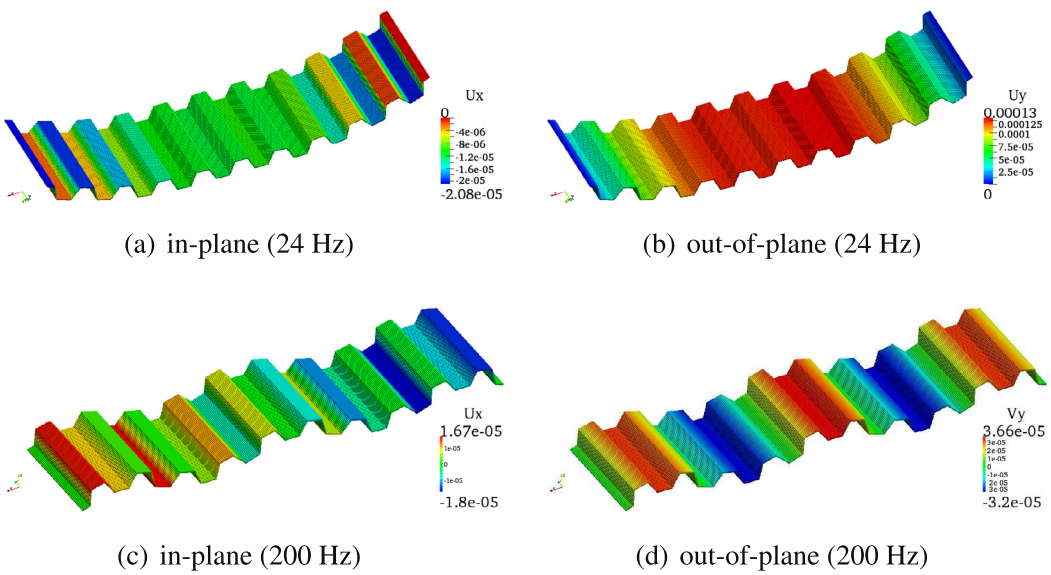

(a) in-plane (24 Hz)

(b) out-of-plane (24 Hz)

(c) in-plane (200 Hz)

(d) out-of-plane (200 Hz)

Fig. 6. Mean deformation shape of the randomly parametrized corrugated panel at 24 Hz and 200 Hz. The colormap of the individual displacement components have been plotted on the deformed panel at that frequency.

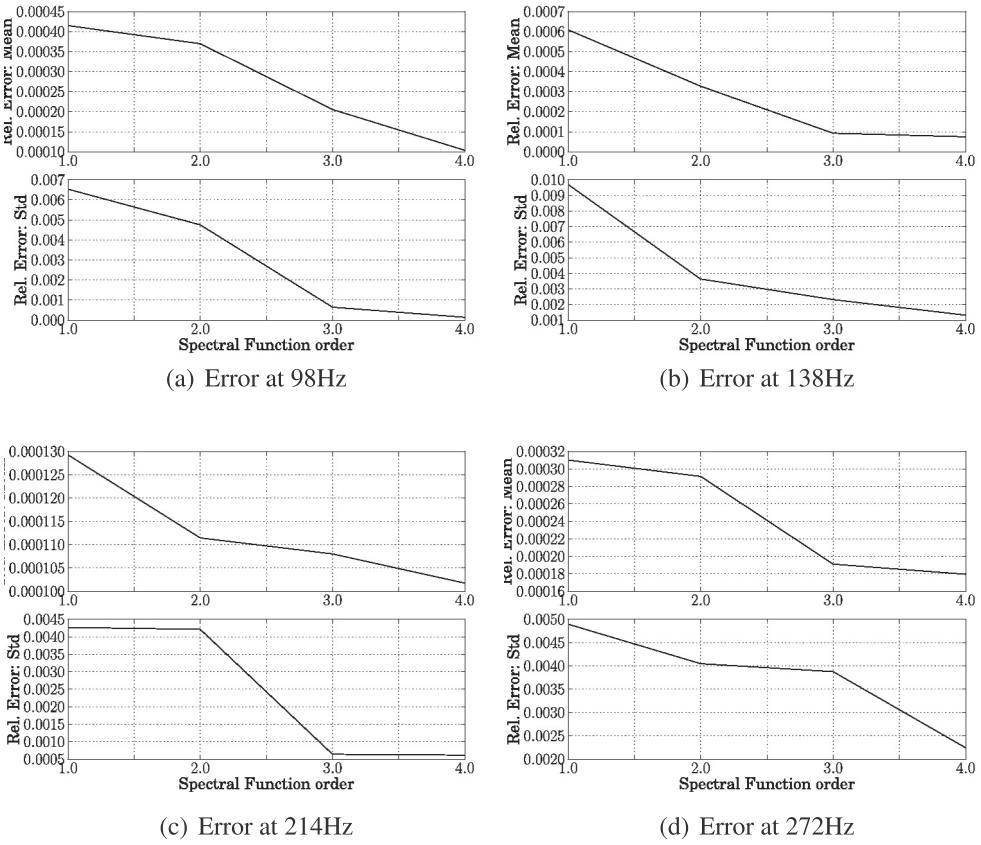

Fig. 7. Convergence trend of the relative error defined with respect to the direct MCS calculations with increasing order of spectral functions at different frequency values.

approximations of the solution are sought, and thus higher order spectral functions are considered. To alleviate the additional computational burden, we use a much smaller sample size and treat them as training runs upon which an emulator of the response is built.

Fig. 6 gives the mean deformation shape of the corrugated panel at two different frequencies (24 Hz and 200 Hz) and plots the colormap of the individual displacement components on the deformed shape. The high frequency deformation shape shows the effect of increased contribution of the higher order structural modes in the response.

A rigorous convergence behavior of the response calculated with increasing order of spectral functions is demonstrated in Fig. 7 which shows the $L2$-relative error norm curves at different values of frequency. The L^2 relative error $\epsilon_{\boldsymbol{\mu}}^{(m)}(\omega)$ is defined at each frequency step ω for mth order spectral functions as

$$\epsilon_{\boldsymbol{\mu}}^{(m)}(\omega) = \frac{\left\| \boldsymbol{\mu}_{SF}^{(m)}(\omega) - \boldsymbol{\mu}_{MCS}(\omega) \right\|_{L^2(\mathcal{D})}}{\left\| \boldsymbol{\mu}_{MCS}(\omega) \right\|_{L^2(\mathcal{D})}}, \tag{44}$$

where $\boldsymbol{\mu}_{SF}^{(m)}(\omega)$ denotes the mean or the standard deviation of the response vector obtained with the spectral weighting functions of order m and $\boldsymbol{\mu}_{MCS}(\omega)$ is the mean or standard deviation of the response vector calculated with direct MCS. We have studied the cases for which $m = 1, \ldots, 4$. Each of Fig. 7(a)–(d) shows two sub-figures, top and bottom, which gives, respectively, the relative error for the calculated mean and standard deviation with the spectral function approach with respect to the direct MCS. It is observed that the solution computed with the higher order spectral function approach provides a better approximation of the direct MCS solution. However, the choice of the spectral function order is constrained by the consideration of the computational cost associated with it.

6.3. Metamodeling

As shown in Fig. 7, the higher the order of the spectral functions, the lower the relative error with respect to direct MCS. This, however, compromises the advantages of the spectral approach due to an increase in computational effort dictated by Eq. (20) and (21). This additional computational cost is mitigated using a Bayesian metamodel (introduced in section 4) to

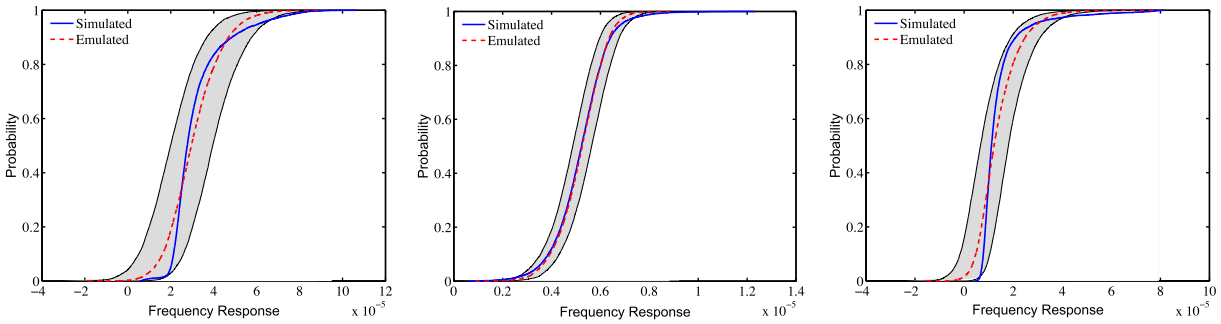

(a) Empirical cdf at 98Hz (b) Empirical cdf at 138Hz (c) Empirical cdf at 214Hz

Fig. 8. Comparison between emulated and simulated cdfs for different frequency levels. 95% credible intervals (shaded areas) are shown for the cdfs.

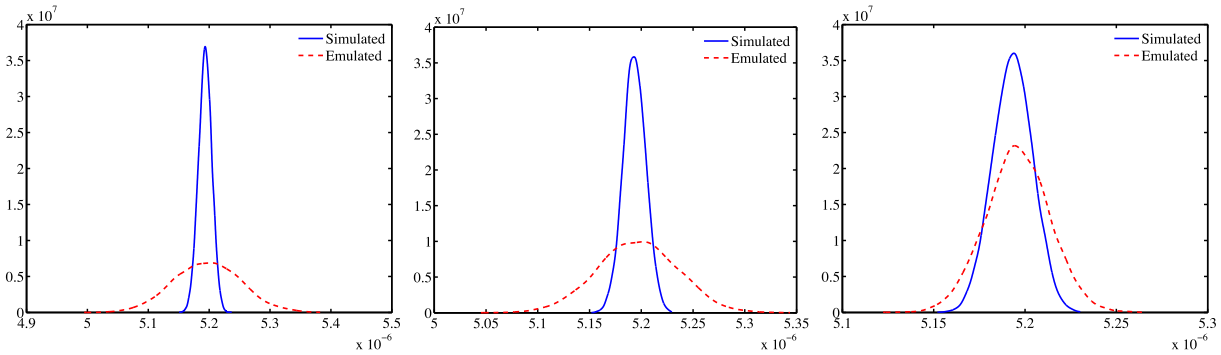

(a) $N = 1000$ (b) $N = 5000$ (c) $N = 10000$

Fig. 9. Simulated vs emulated mean of the sample distribution. As the number of random functions generated with Algorithm 3 increases, the variance of the sample mean decreases. This means that uncertainty about the sample mean results from the lack of information due to the computational cost of the original simulator.

obtain the statistics of the stochastic sample response approximated with finite order spectral functions. Given our choice of correlation length, we follow the suggestion in [50] and generate a set of 250 training runs (corresponding to the 25 random variables in the KL expansion). In terms of Algorithm 1, for every frequency level ω, a sample of design points $\{\boldsymbol{\xi}^{(1)}, \ldots, \boldsymbol{\xi}^{(250)}\}$ is generated using a space-filling strategy, such as a Latin hypercube. Each design point is drawn from the input distribution $\mathcal{F}(\boldsymbol{\xi})$, a multivariate standard normal random variable in a 25-dimensional space. The design points are evaluated and the corresponding system response is reconstructed. The resulting training runs for each frequency level are of the form $(\boldsymbol{\xi}^{(i)}, \hat{u}_k^{(m)}(\boldsymbol{\xi}^{(i)}))$ for $i = 1, \ldots, 250$. Once the training runs are generated, they are passed to Algorithm 2, where the posterior mean and covariance are computed, and thus the posterior distribution in Eq. (36) can be specified. As mentioned before, the posterior mean can be used as an approximation to the simulator's output. Fig. 8 exemplifies the accuracy of such an approximation for some fixed frequency levels. In particular, it shows a comparison between the cumulative distribution functions (cdfs) generated with 10,000 Monte Carlo simulations and the cdfs obtained by emulation based on 250 training runs. 95% credible intervals for the emulated cdfs are also displayed. The advantages of Bayesian emulation become apparent: while every MCS run is independent, Bayesian emulation takes advantage of the information that each design point contains about the nearest design points. This information is contained in the covariance structure in Eq. (30).

Once the posterior distribution has been computed using Algorithm 2, any statistical summary of the output distribution can be estimated by Algorithm 3. A large sample is drawn from the input distribution $\mathcal{F}(\boldsymbol{\xi})$ and samples generated from the posterior distribution are used to estimate the summary. The process is illustrated in Fig. 9, where samples of increasing size are drawn from the posterior distribution in order to estimate the mean of the output distribution. The prediction is contrasted with 10,000 Monte Carlo samples. It can be seen how the variance of the sample mean estimated via Bayesian emulation is reduced. Note however that this variance will always be greater than the Monte Carlo variance, since the emulator is built upon a finite number of training runs, and there will always be a lack of information due to this smaller set of simulator evaluations. It is therefore important to understand that our uncertainty about the mean is not due to Monte Carlo error, but due to lack of information due to the computational cost of the simulator.

The analysis described above was repeated across the entire frequency range of 0–300 Hz. For every frequency level ω, the Bayesian uncertainty analysis was performed and statistics of the FRF were obtained. Fig. 10 shows the emulated mean and standard deviation of the FRF.

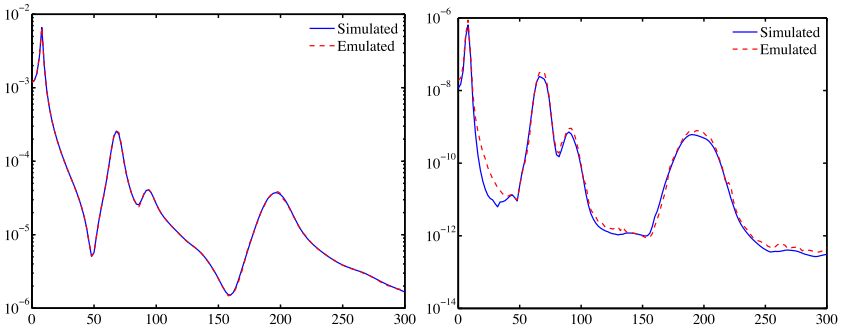

Fig. 10. Emulation and simulation of the mean frequency response (a) and variance of the frequency response (b). The simulation was performed for every frequency level in the input domain, based on 10,000 samples. Only 250 samples were necessary to emulate the statistics of the frequency response at a comparable accuracy.

7. Conclusions

The stochastic vibration response of a randomly parametrized structural dynamic system has been considered in this paper. The system response has been evaluated with a hybrid spectral and metamodeling approach which provides a computationally efficient scheme of parametric uncertainty propagation to the system response. In the first step, the system response is resolved at random points in the stochastic input space using the spectral function approach which relies on stochastic Krylov basis functions and the projection of the solution onto a reduced space of structural modes of the vibrating system and a set of stochastic spectral weighting functions. Then the evaluated response at these random samples provide training runs which are used by a Bayesian metamodel, which emulates the system response in order to estimate the uncertainty distribution and derive response statistics across the frequency range. The principal contributions of the work presented here can be summarized as follows:

- The spectral functions, constructed with an 'equivalent' Neumann type series expansion with preconditioned stochastic Krylov basis functions, in conjunction with a reduced modal subspace projection scheme offers an efficient way of propagating the uncertainty associated with randomly parametrized systems.
- The proposed solution methodology is more efficient compared to the crude Monte Carlo simulation.
- The finite order spectral functions are highly non-linear rational functions of the input stochastic variables used to model the parametric uncertainty.
- Higher order spectral functions produce a more accurate approximation of the stochastic system response but are computationally more expensive.
- A Bayesian emulator can be used to reduce the cost associated with an increasing order of spectral functions. Samples drawn from the posterior distribution can be used to perform uncertainty analysis of the response.
- A corrugated panel with random elastic parameters has been analyzed with the proposed approach. This might contribute to the understanding of the dynamic behavior of this type of structure and their use in future applications of morphing aircraft.
- The response curves obtained with the spectral function and the direct MCS method are in good agreement even near the resonance frequencies.
- The relative error plots show an increase in the accuracy of the approximated solution when using higher order spectral functions.
- A statistical summary of the system response, such as the mean or the standard deviation, can be emulated, whenever a Monte Carlo estimate is not feasible.

These results demonstrate the applicability and computational efficacy of the stochastic spectral function approach in conjunction with the Bayesian emulator proposed in this work and has been demonstrated for a corrugated panel with random elastic parameters. The applicability of the method stems from the enhanced accuracy of the approximate solution obtained due to the use of carefully chosen stochastic preconditioners.

Future work along this direction may extend the underlying idea of the methodology presented here to the case of transient time domain response of stochastic dynamical systems. Also, when considering non-linear dynamical problems, where the uncertainty propagation methods tend to become more complicated and computationally intensive, the proposed method can be used to significant advantage. For example, the proposed spectral approach can be used at every linearization step of the iterative technique required in the response evaluation. While the increase in spectral order increases the accuracy of the approximated solution, the choice of the optimum order of spectral functions is not obvious from the relative error analysis results presented here and there is scope to introduce adaptivity, based on some a posteriori error estimators.

Acknowledgements

AK acknowledges the financial support from Swansea University through the award of the Zienkiewicz scholarship. SA acknowledges the financial support from The Royal Society of London through the Wolfson Research Merit Award. MIF acknowledges funding from the European Research Council through Grant No. 247045 entitled "Optimisation of Multi-scale Structures with Applications to Morphing Aircraft".

References

[1] H.G. Matthies, Uncertainty quantification with stochastic finite elements, Encyclopedia of Computational Mechanics, Wiley Online Library, 2007.
[2] M. Papadrakakis, V. Papadopoulos, Robust and efficient methods for stochastic finite element analysis using Monte Carlo simulation, Comput. Methods Appl. Mech. Eng. 134 (3–4) (1996) 325–340.
[3] H.J. Pradlwarter, G.I. Schuëller, On advanced Monte Carlo simulation procedures in stochastic structural dynamics, Int. J. Non-linear Mech. 32 (4) (1997) 735–744 (Third International Stochastic Structural Dynamics Conference).
[4] M. McKay, W. Conover, R. Beckman, A comparison of three methods for selecting values of input variables in the analysis of output from a computer code, Technometrics 21 (2) (1979) 239–245.
[5] M. Kleiber, T.D. Hien, The Stochastic Finite Element Method, Wiley, New York, USA, 1992.
[6] F. Yamazaki, M. Shinozuka, G. Dasgupta, Neumann expansion for stochastic finite element analysis, J. Eng. Mech.-ASCE 114 (8) (1988) 1335–1354.
[7] H.G. Matthies, A. Keese, Galerkin methods for linear and nonlinear elliptic stochastic partial differential equations, Comput. Methods Appl. Mech. Eng. 194 (12–16) (2005) 1295–1331.
[8] C. Pettit, P. Beran, Spectral and multiresolution wiener expansions of oscillatory stochastic processes, J. Sound Vibr. 294 (45) (2006) 752–779.
[9] R. Ghanem, P.D. Spanos, Stochastic Finite Elements: A Spectral Approach, Springer-Verlag, New York, USA, 1991.
[10] D. Xiu, G.E. Karniadakis, The Wiener–Askey polynomial chaos for stochastic differential equations, SIAM J. Sci. Comput. 24 (2) (2002) 619–644.
[11] A. O'Hagan, Bayesian analysis of computer code outputs: a tutorial, Reliab. Eng. Syst. Safety 91 (10–11) (2006) 1290–1300.
[12] J. Sacks, W. Welch, T. Mitchell, H. Wynn, Design and analysis of computer experiments, Stat. Sci. 4 (4) (1989) 409–435.
[13] T. Santner, B. Williams, W. Notz, The Design and Analysis of Computer Experiments, Springer Series in Statistics, Springer, London, UK, 2003.
[14] F.A. DiazDelaO, S. Adhikari, Structural dynamic analysis using Gaussian process emulators, Eng. Comput. 27 (5) (2010) 580–605.
[15] E.I. Saavedra Flores, F.A. DiazDelaO, M.I. Friswell, J. Sienz, A computational multi-scale approach for the stochastic mechanical response of foam-filled honeycomb cores, Compos. Struct. 94 (5) (2012) 1861–1870.
[16] F.A. DiazDelaO, S. Adhikari, Gaussian process emulators for the stochastic finite element method, Int. J. Numer. Methods Eng. 87 (6) (2011) 521–540.
[17] F.A. DiazDelaO, S. Adhikari, Bayesian assimilation of multi-fidelity finite element models, Comput. Struct. 92–93 (2012) 206–215.
[18] A. Bobrowski, Functional Analysis for Probability and Stochastic Processes: An Introduction, Cambridge Univ. Press, 2005.
[19] I. Babuška, R. Tempone, G.E. Zouraris, Galerkin finite element approximations of stochastic elliptic partial differential equations, SIAM J. Numer. Anal. 42 (2) (2004) 800–825.
[20] R. Ghanem, D. Ghosh, Efficient characterization of the random eigenvalue problem in a polynomial chaos decomposition, Int. J. Numer. Methods Eng. 72 (2007) 486–504.
[21] S. Adhikari, Joint statistics of natural frequencies of stochastic dynamic systems, Comput. Mech. 40 (4) (2007) 739–752.
[22] S. Adhikari, Calculation of derivative of complex modes using classical normal modes, Comput. Struct. 77 (6) (2000) 625–633.
[23] A. Nouy, Generalized spectral decomposition method for solving stochastic finite element equations: invariant subspace problem and dedicated algorithms, Comput. Methods Appl. Mech. Eng. 197 (51–52) (2008) 4718–4736.
[24] P.B. Nair, A.J. Keane, Stochastic reduced basis methods, AIAA J. 40 (8) (2002) 1653–1664.
[25] S. Adhikari, A reduced spectral function approach for the stochastic finite element analysis, Comput. Methods Appl. Mech. Eng. 200 (21–22) (2011) 1804–1821.
[26] L. Pichler, H. Pradlwarter, G. Schueller, A mode-based meta-model for the frequency response functions of uncertain structural systems, Comput. Struct. 87 (5–6) (2009) 332–341.
[27] B. Goller, H. Pradlwarter, G. Schuller, An interpolation scheme for the approximation of dynamical systems, Comput. Methods Appl. Mech. Eng. 200 (1–4) (2011) 414–423.
[28] B.V. den Nieuwenhof, J.-P. Coyette, Modal approaches for the stochastic finite element analysis of structures with material and geometric uncertainties, Comput. Methods Appl. Mech. Eng. 192 (33–34) (2003) 3705–3729.
[29] G. Falsone, G. Ferro, An exact solution for the static and dynamic analysis of FE discretized uncertain structures, Comput. Methods Appl. Mech. Eng. 196 (21–24) (2007) 2390–2400.
[30] A. Sarkar, R. Ghanem, Mid-frequency structural dynamics with parameter uncertainty, Comput. Methods Appl. Mech. Eng. 191 (47–48) (2002) 5499–5513.
[31] R.G. Ghanem, R.M. Kruger, Numerical solution of spectral stochastic finite element systems, Comput. Methods Appl. Mech. Eng. 129 (3) (1996) 289–303.
[32] A. Keese, H.G. Matthies, Hierarchical parallelisation for the solution of stochastic finite element equations, Comput. Struct. 83 (14) (2005) 1033–1047.
[33] G. Blatman, B. Sudret, An adaptive algorithm to build up sparse polynomial chaos expansions for stochastic finite element analysis, Probab. Eng. Mech. 25 (2) (2010) 183–197.
[34] X. Wan, G.E. Karniadakis, An adaptive multi-element generalized polynomial chaos method for stochastic differential equations, J. Comput. Phys. 209 (2) (2005) 617–642.
[35] E.J. Grimme, Krylov projection methods for model reduction (Ph.D. thesis), University of Illinois at Urbana-Champaign, 1997.
[36] V. Kozyakin, On accuracy of approximation of the spectral radius by the Gelfand formula, Linear Algebra Appl. 431 (11) (2009) 2134–2141.
[37] J.E. Oakley, A. O'Hagan, Probabilistic sensitivity analysis of complex models: a Bayesian approach, J. R. Stat. Soc. B 66 (3) (2004) 751–769.
[38] A. O'Hagan, Some Bayesian numerical analysis, Bayesian Statistics, vol. 4, Oxford University Press, Cambridge, UK, 1992. pp. 345–363.
[39] R. Haylock, A. O'Hagan, On inference for outputs of computationally expensive algorithms with uncertainty on the inputs, Bayesian Statistics, vol. 5, Oxford University Press, Oxford, UK, 1996.
[40] J. Oakley, Eliciting Gaussian process priors for complex computer codes, The Statistician 51 (1) (2002) 81–97.
[41] J. Rougier, Probabilistic inference for future climate using an ensemble of climate model evaluations, Clim. Change 81 (3) (2007) 247–264.
[42] J.E. Oakley, A. O'Hagan, Bayesian inference for the uncertainty distribution of computer model outputs, Biometrika 89 (2002) 769–784.
[43] T.E. Fricker, J.E. Oakley, N.D. Sims, K. Worden, Probabilistic uncertainty analysis of an FRF of a structure using a Gaussian process emulator, Mech. Syst. Signal Process. 25 (8) (2011) 2962–2975.
[44] R.B. Lehoucq, D.C. Sorensen, C. Yang, ARPACK users' guide: solution of large-scale eigenvalue problems with implicitly restarted Arnoldi methods, SIAM 6 (1998).
[45] I. Vernon, M. Goldstein, R.G. Bower, Galaxy formation: a Bayesian uncertainty analysis, Bayesian Anal. 5 (4) (2010) 619–670.
[46] S. Barbarino, O. Bilgen, R.M. Ajaj, M.I. Friswell, D.J. Inman, A review of morphing aircraft, J. Intell. Mater. Syst. Struct. 22 (9) (2011) 823–877.
[47] Y. Xia, M.I. Friswell, E.I. Saavedra Flores, Equivalent models of corrugated panels, Int. J. Solids Struct. 49 (13) (2012) 1453–1462.

[48] I. Dayyani, S. Ziaei-Rad, H. Salehi, Numerical and experimental investigations on mechanical behavior of composite corrugated core, Appl. Compos. Mater. 19 (2012) 705–721.
[49] C.E. Powell, H.C. Elman, Block-diagonal preconditioning for spectral stochastic finite-element systems, IMA J. Numer. Anal. 29 (2) (2009) 350–375.
[50] J. Loeppky, J. Sacks, W. Welch, Choosing the sample of a computer experiment: a practical guide, Technometrics 51 (2009) 366–376.